A STUDY OF THE STANDARD CIRRUS WING LIFT DISTRIBUTION VERSUS BELL-SHAPED

LIFT DISTRIBUTION

A Thesis

presented to

the Faculty of California Polytechnic State University,

San Luis Obispo

In Partial Fulfillment

of the Requirements for the Degree

Master of Science in Aerospace Engineering

by

William H. Bergman

June 2020

COMMITTEE MEMBERSHIP

TITLE: A Study of the Standard Cirrus Wing Lift Distribution

                                    Versus Bell Shaped Lift Distribution

AUTHOR: William H. Bergman

DATE SUBMITTED: June 2020

COMMITTEE CHAIR: Aaron Drake, Ph.D.

                                    Professor of Aerospace Engineering

COMMITTEE MEMBER: Paulo Iscold, Ph.D.

                                    Associate Professor of Aerospace Engineering

COMMITTEE MEMBER: Arnold Deffo, Ph.D.

                                    Assistant Professor of Aerospace Engineering

COMMITTEE MEMBER: Russell Westphal, Ph.D.

                                    Professor of Mechanical Engineering

ABSTRACT

A Study of the Standard Cirrus Wing Lift Distribution Versus Bell Shaped Lift Distribution

William H. Bergman

This thesis discusses a comparison of the differences in aerodynamic performance of wings designed with elliptical and bell-shaped lift distributions. The method uses a Standard Cirrus sailplane wing with a lift distribution associated with the induced drag benefits of an elliptical distribution (span efficiency = 0.96) as the basis of comparison. The Standard Cirrus is a standard class sailplane with 15-meter wingspan that was designed by Schempp-Hirth in 1969. This sailplane wing was modeled and analyzed in XFLR5, then validated against existing wind tunnel airfoil data, and Standard Cirrus flight test data. The root bending moment of the baseline wing was determined and used as the primary constraint in the design of two wings with bell-shaped lift distribution. These wings were modeled in XFLR5 by adjusting chord length and geometric twist respectively, and then they were studied using fixed speed lifting line analysis. Steady state cruise conditions for the Standard Cirrus sailplane were taken from the flight test data and applied for the analysis.

The wing designed with chord variation posed incompatibilities with the lifting line method. The resulting planform was strongly tapered in the wingtip region and the reference chord length there was such that the software could not solve for a Reynolds number the magnitude resulting from two-dimensional airfoil analysis. However, the wing geometry provided insight into the design aspect of wings with bell-shaped lift distribution. Using chord variation to shape the lift distribution, the wing featured a 12% increase in wingspan but a 6.5% decrease in total wetted area when compared to the baseline.

The results of the analysis of the wing designed with geometric twist indicate that induced drag decreased by 5% when compared to the baseline wing. The constraint on root bending moment resulted in a 12% increase in wingspan. Wetted area also increased by 14.8% over the baseline yielding an estimated 15% increase in skin friction.

ACKNOWLEDGMENTS

I would like to acknowledge Dr. Drake for giving me guidance throughout my time at Cal Poly both with thesis work and in my general approach to life. He listened to my whimsical ideas and even still offered me a place in the aerospace program and in his lab. Between office hours and trips out to the EFR, he has taught me to be a more logical thinker through his healthy skepticism and sharp sense of humor.

My committee members have also been a great source of learning over my two years in San Luis Obispo. Thank you Dr. Westphal for spending your office hours talking to me about history and compressible flow during my first quarter at the university. You made me feel welcome in a new environment. Dr. Iscold, thank you for taking me along on the GVT test for Nixus and for being a spring of inspiration with your achievements. Dr. Deffo, I regret not getting further into the structural considerations of this work, but I would like to continue research in the future and would be grateful for your mentorship there if you would permit it.

Thank you, Al Bowers, for providing me with the initial spark that lead me down this path. Your technical note from 2016 exposed me to theoretical aerodynamics and a greater appreciation of nature. It also motivated me to go back to school and learn a great deal beyond my intended research.

I would like to also acknowledge my friends and family for supporting me always in all aspects of life. I am fortunate for winding up at 338 where I made friendships that I could never have imagined before moving to SLO. Rest in peace Don and thank you for building such a strange place to call home.

Finally, I would like to dedicate this thesis to my grandfather Dr. Gunnar Bergman whose curiosity could never be snuffed out. The flame burns on in your name.

TABLE OF CONTENTS

LIST OF TABLES

LIST OF FIGURES

Chapter 1

INTRODUCTION

In 1920 Ludwig Prandtl [1] developed lifting line theory to approach the problem of determining what lift distribution over the span of a wing should produce the lowest induced drag. Prandtl first bounded the problem by using a straight wing of uniform airfoil and fixed span. With the span constrained, he found that an elliptically shaped lift distribution yields the least induced drag.

In 1933 however, he approached the problem differently by instead constraining overall wing structural loading [2]. Once again, he applied his lifting line theory to solve for the resulting lift distribution and found that it took on a bell shape. The natural follow-up question was how the two lift distributions compare to each other in terms of minimum induced drag.
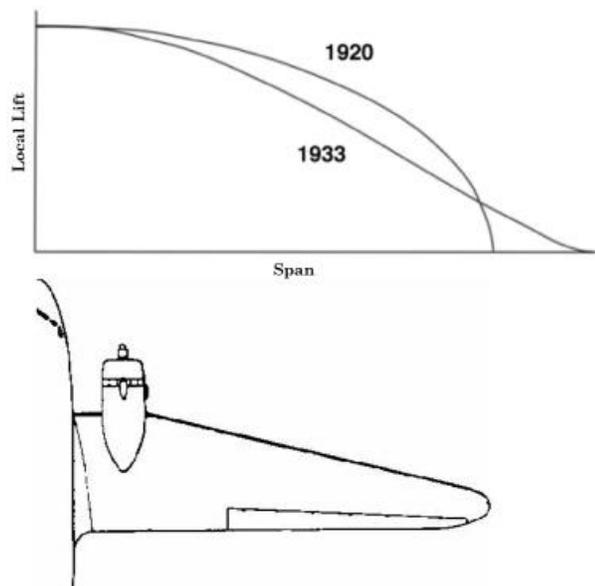
Figure 1.1: An illustration of elliptical versus bell-shaped local lift distributions over a semi-span.

1.1 Statement of Problem

This thesis aimed to answer this question by comparing three wings: an existing wing with a lift distribution designed with minimized induced drag associated with elliptical loading, and two with bell shaped lift distribution. These comparisons used a Standard Cirrus sailplane wing as the baseline. Two wings with bell-shaped loading were then designed using the same bending moment as the baseline wing, and the same total lift. To apply the structural loading constraint on the bell wing, the root bending moment was fixed between all the wing designs.

Figure 1.2: Standard Cirrus sailplane [3].

1.2 Purpose of Research

Aircraft wing design is influenced by a wide range of considerations for the overall system, but one factor that is generally sought to be minimized is that of induced drag. Rising fuel costs and burgeoning air travel around the world have driven commercial aircraft manufacturers to optimize their fleets for fuel efficiency. Aerodynamic improvements to the fuselage and lifting surfaces of airplanes have provided incremental gains in efficiency over recent decades. Varying wing geometry to achieve different spanwise lift distributions is one aspect of design that could yield a reduction in fuel consumption through a reduction in induced drag. This thesis focuses on directly

comparing elliptical and bell-shaped lift distributions as they affect the aerodynamic efficiency of a specific baseline aircraft. The lessons learned from this exercise aim to better the understanding of how a bell-shaped lift distribution affects induced drag.

1.3 Literature Review

This section reviews previous theoretical work done on the comparison of drag induced by elliptical and bell-shaped lift distributions. It also details different methods to apply constraints on total lift and wing structure to set up the comparison. Information on the Standard Cirrus sailplane geometry and performance are also provided.

1.3.1 The Original Prandtl Theory

Ludwig Prandtl developed lifting line theory to approach the problem of determining the lift distribution of a wing of minimum induced drag. The problem is classically set up by constraining gross weight and wingspan. Doing so yields an elliptical lift distribution (ELD) which Prandtl published in 1919 [1]. Prandtl later discovered that there exists a lift distribution of 11% lower induced drag and 22% greater span that can be determined by constraining different parameters. In the case of the so-called bell-shaped lift distribution (BSLD) published in 1933, Prandtl instead fixed the structural weight by constraining the moment of inertia of the theoretical lift-distribution as follows [2].

The expressions for induced drag, total lift, and moment of inertia of the lift-distribution are given as functions of the spanwise coordinate below [5].

$$D_i = 4\rho_\infty V_\infty^2 b^2 \int_0^1 w(y)\alpha_i(y)dy \qquad (1)$$

$$L = 2\rho_\infty V_\infty^2 b^2 \int_0^1 w(y)dy \tag{2}$$

$$Lr^2 = 2\rho_\infty V_\infty^2 b^4 \int_0^1 w(y)y^2 \, dy \tag{3}$$

where ρ_∞ is air density, V_∞ is free stream velocity, b is the wingspan, $w(y)$ is downwash as a function of spanwise location y, r is the radius of gyration, and α_i is induced angle of attack which will be further explained in the next chapter. To optimize for the minimum induced drag, the differential terms of equations 1-3 are first derived, then set equal to zero.

$$\delta D_i = 2 \int_0^1 \delta w(y)\alpha_i(y)dw = 0 \tag{4}$$

$$\delta L = \int_0^1 \delta w(y)dy = 0 \tag{5}$$

$$\delta Lr^2 = \int_0^1 \delta w(y)y^2 \, dy = 0 \tag{6}$$

After solving for an explicit expression for $w(y)$, and substituting this in the equation for induced drag (Eq.1), the result can be compared to the amount of drag induced by an elliptical wing of equivalent total lift, D_{ie}, using the ratio of their wingspans, σ.

$$\frac{D_i}{D_{ie}} = \frac{4\sigma^4 - 6\sigma^2 + 3}{\sigma^6} \tag{7}$$

The minimum of the ratio of induced drags, 0.89, occurs at a σ of 1.22 – that is to say that the drag induced by the bell wing is 11% less than the elliptical wing of equivalent total lift and moment of inertia of lift-distribution, when the span of the bell wing is 22% longer. Given the

potential advantages of further reducing induced drag, this theory has since been revisited and reformulated by other aerodynamic researchers.

Al Bowers, in 2016 published a technical note that expanded on Prandtl's theory and drew further conclusions about the nature of wings with BSLD [15]. He stated that in contrast to the sharp discontinuity in downwash at the wingtips of an elliptically loaded wing, the downwash curve of a bell-loaded wing should feature a smooth and continuous transition to upwash at 70.4% semi-span. It follows that the outboard 29.6% of the wingspan in the upwash region should experience induced thrust. He explains that the placement of an aileron control surface in this part of the wing yields the potential for coordinated turns without the need for a rudder because aileron deflection would result in a corresponding yaw moment in the coordinated direction.

To the author's knowledge, a one-to-one performance comparison between wings of ELD and BSLD does not currently exist. The goal of this thesis project is to use a Standard Cirrus Sailplane as a basis of comparison between the two distributions. Ultimately a wing with BSLD will be designed and analyzed using panel codes to provide metrics of comparison between key performance data. The first step, however, is to develop a firm understanding of the underlying theory and previous work on the topic. This literature review provides a summary of several resources that present different approaches to determining the lift distribution of minimum induced drag that will be considered to help guide the course of research.

1.3.2 Constraining Total Lift and Root Bending Moment

Several resources have been identified that approach the problem by fixing total lift and root bending moment. The motivation for this approach stems from the relationship between the weight of the wing spars and the local bending moment due to aerodynamic forces at each wing section. The wing structure must be designed such that it can withstand the aerodynamic loads that it is subjected to. Wing structural weight is desired to be kept at a minimum however so that overall aircraft weight can be minimized. Therefore, the root bending moment of the wing provides a good starting point for optimization because it reflects the sum of aerodynamic forces

along the span of the wing which have a direct correlation to the structural weight of the wing assuming that the spar is the primary structural element [17].

R.T. Jones [4] in 1950 published a paper that provides an analytical comparison between wings of BSLD and ELD with the above constraints applied to both while allowing span to vary. His formulation, much like Prandtl led to a system of differential expressions for elements of lift, and induced drag and bending moment (rather than moment of inertia of lift distribution).

$$\delta L = 0, \qquad l_1 + l_2 + l_3 = 0 \tag{8}$$

$$\delta M_R = 0, \qquad l_1 y_1 + l_2 y_2 + l_3 y_3 = 0 \tag{9}$$

$$\delta D_i = 0, \qquad l_1 w_{i1} + l_2 w_{i2} + l_3 w_{i3} = 0 \tag{10}$$

from which a system of linear equations can be derived to satisfy the conditions where

$$w_i \propto a + by \tag{11}$$

such that a and b are constants. This expression for downwash suggests that for the given constraints, "the downwash must show linear variation along the span." The Jones paper also provides an explicit form for the induced drag associated with his approach:

$$D_i = \frac{L^2}{\pi \frac{\rho_\infty}{2} V_\infty (2b_e)^2} [8\sigma^4 - 16\sigma^3 + 9\sigma^2]. \tag{12}$$

This equation contains the expression for induced drag of an ELD (outside the brackets) with the addition of several scaling factors that contain the ratio of the semi-span of the wing to that of an ELD having the same total lift and bending moment, σ. Minimizing this equation, the induced drag is found to be 15% less than the elliptical baseline, when the span of the bell wing is allowed to extend to 15% longer than the baseline.

A. Klein and S.P. Viswanathan [5] took a similar approach to the problem in their paper by solely constraining the root bending moment. They also employed an analytical method starting with a review of Prandtl's original formulation. Then, they replaced the terms for moment of inertia of the lift-distribution (Eq. 3), and the differential element of moment of inertia (Eq. 6) with the corresponding terms for root bending moment M_R.

$$M_R = 2\rho_\infty V_\infty^2 b^3 \int_0^1 \gamma(\eta)\eta \, d\eta \qquad (13)$$

$$\delta M_R = \int_0^1 \delta\gamma(\eta)\eta \, d\eta = 0 \qquad (14)$$

After solving with these boundary conditions, they found an explicit expression for the induced drag which, like the Jones approach, also contains the elliptical induced drag with a scaling factor.

$$\frac{D_i}{D_{ie}} = \frac{\sigma^2 + 8(1 - \sigma^2)}{\sigma^4} \qquad (15)$$

The minimum ratio of induced drag in this case was 0.844 with a wingspan ratio of 1.33. This means that replacing Prandtl's original constraint with that of the root bending moment yielded a roughly 16% reduction in induced drag with a 33% increase in span compared to an elliptical baseline.
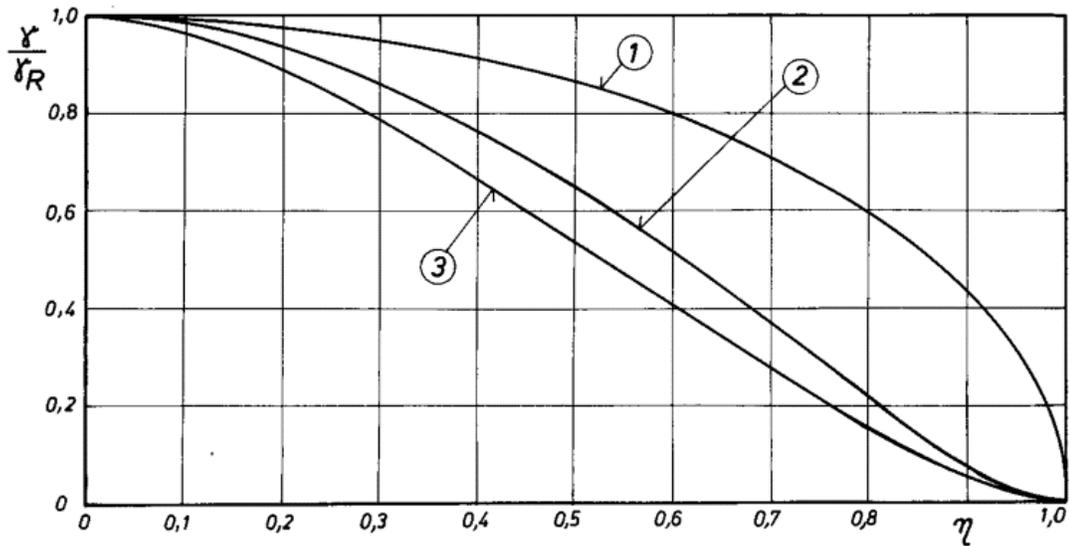
Figure 1.3: Comparison of three spanwise wing loadings: 1 – elliptical, 2 – Prandtl's bell, 3 – Klein & Viswanathan 1973 [5].

Despite doubling the wingspan over the wing discussed in the Jones paper, Klein & Viswanathan concluded on only 1% greater savings on induced drag. This result appears to follow suit with a point made in the Jones paper that extending the wingspan past 15% leads to diminishing and marginal reductions in induced drag. They also included figures that illustrate both a comparison of the spanwise lift distribution curves, and induced drag ratio versus span ratio of Prandtl and his solutions. This curve shows that the bending moment constraint led to further reductions in induced drag than the moment of inertia of lift distribution constraint. It also shows that past the optimized wingspan, further increasing the span does in fact lead to diminishing improvements in induced drag.

Two years later the same pair of Klein and Viswanathan [6] took a novel approach at the optimization problem by constraining wing structural weight with integrals of the spanwise shear-force and bending moment distributions. They start with the integrals used in determining the spanwise shear force and bending moment due to air loads. Then the spanwise loadings are determined for which the induced drag is given as a function of spanwise flow angles and loadings. This yields an expression with three constants that are solved for by applying the

8

structural constraints, resulting in an induced drag ratio of 0.929 with a span ratio of 1.160. This result is compared to the Prandtl paper, and the previous result found by this research team on a plot of induced drag ratio versus span ratio using the classical ELD as the basis. The results from this paper indicate a 7% reduction in reduced drag with a 16% increase in span. The conclusion discusses the range of possible lift distributions that are possible by constraining different aspects of the wing design.
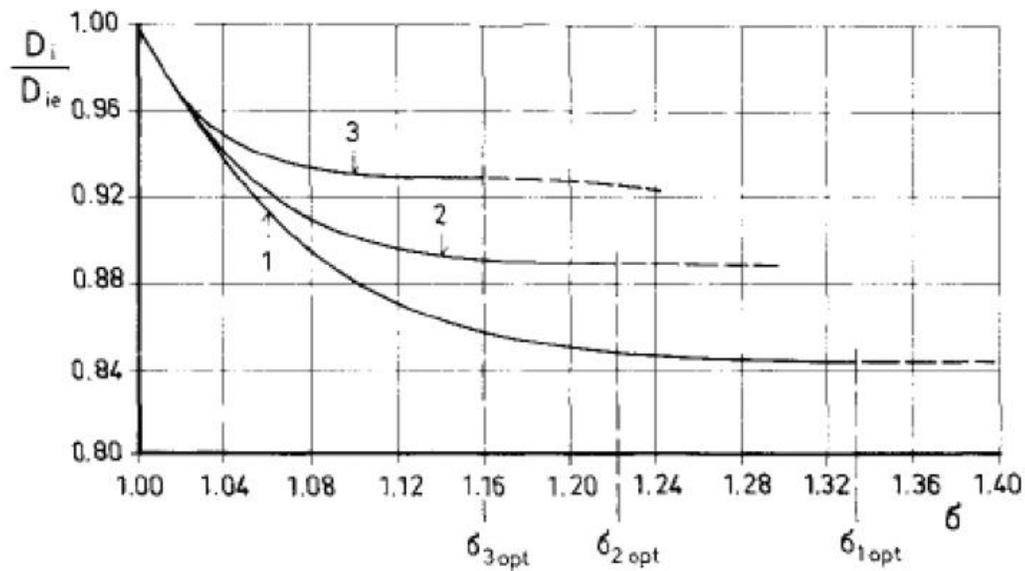
Figure 1.4: Bell/elliptical Induced drag ratio versus span-ratio for three different bell wing loadings: 1 – Prandtl, 2 – Klein & Viswanathan (1973), 3 – Klein & Viswanathan (1975) [6].

Phillips, Hunsaker and Joo [7] take analysis a step further and consider three cases to arrive at minimum induced drag: 1) fixed weight, max stress, and chord length, 2) fixed weight, max stress, and wing loading, and 3) fixed weight, max deflection, and wing loading. Their approach yielded a formulation resulting from Fourier analysis where all the lift distributions could be obtained by varying the coefficient of one the Fourier terms. The report concludes that stress-limited designs would excel in high load factor maneuvers whereas elliptical distributions still induce the least amount of drag in steady level flight. It offers the design consideration of employing variable twist geometries to transition between lift distributions. The deflection-limited solution resulted in a significant 16.5% increase in induced drag. However, the paper states that

this conclusion was reached simply to demonstrate a method of deriving lift distribution from fixed deflection and that other approaches might be more suitable in practice.

It should be mentioned that all the papers discussed to this point have employed analytical methods for determining lift distribution. They are highly theoretical and apply only to wings of rectangular, un-swept planform. There are certainly other ways of achieving BSLD such as allowing for variable chord length or spanwise twist. After obtaining a thorough understanding of the analytical methods employed in the above papers, this research will use a numerical panel code to investigate BSLD developed through variable chord length and geometric twist. These additional variable design parameters will allow for a more practical approach to the comparison of lift distributions.

1.3.3 Standard Cirrus Sailplane Baseline

Thomas Hansen [8] produced a comprehensive analysis of the performance of the Standard Cirrus sailplane. He used Idaflieg flight test results to validate extensive simulations run in CFD. This report will likely be used as a basis of comparison to the wing of BSLD that is ultimately designed. CFD does not provide an easy way to determine induced drag however, so the wing geometry will be adapted to panel codes for that calculation. Fortunately, Hansen has provided the CAD geometry for the sailplane that he made using a digitizing arm. The CFD physics parameters used in his report have also been supplied so that consistent simulations can be run for performance comparison.

1.3.4 Summary

There was found to be significant variation in results across the different approaches taken to calculate the induced drag of BSLD. Constraining different parameters yielded a wide spectrum of results but there was a consistent overall reduction in induced drag with the BSLD.

Chapter 2

APPROACH AND METHODOLOGY

2.1 XFLR5

Version 6.47 of XFLR5 was chosen to carry out the theoretical aerodynamic analysis of both two- and three-dimensional geometries. This software was selected because it is intended for airfoil and wing analysis at low Reynolds numbers using lifting line theory with a panel method. In fact, XFLR5 was originally developed to model the performance of sailplanes and is additionally open for free public use. While lifting line theory does not consider compressible flow effects, those factors lie outside of the scope of this thesis which focuses on an inviscid comparison of lift distributions.

2.1.1 Governing Equations of Lifting Line Theory

The governing equations of lifting line theory were derived by Ludwig Prandtl during 1911-1918 [9] when he further developed the vortex filament model of a wing. The model discretizes the circulation about a wing into an infinite number of vortex filaments that both extend to infinity off the trailing edge in the direction of the freestream flow and are fixed to the flow with a common bound vortex.
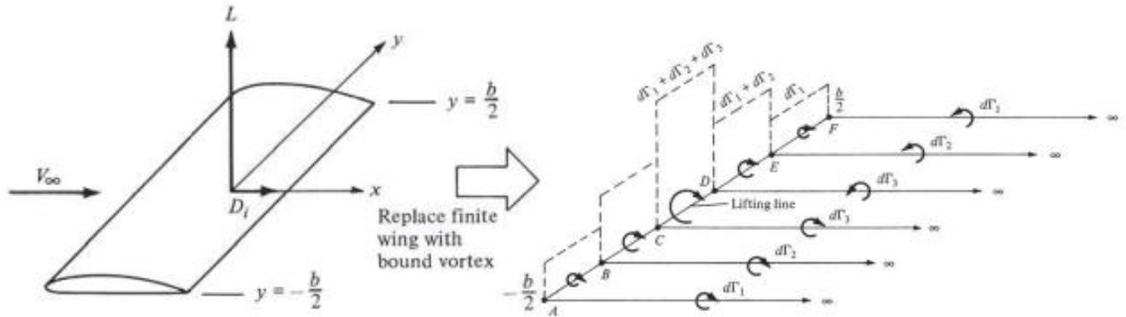
Figure 2.1: Depiction of the vortex filament model of a finite wing. [9]

Following from the work done by his contemporaries, a bound vortex should experience a force expressed by the Kutta-Joukowski equation:

$$L'(y_0) = \rho_\infty V_\infty \Gamma(y_0) \tag{16}$$

where $L'(y_0)$ is the local lift force acting at a location along the span, ρ_∞ is the freestream density, V_∞ is the freestream velocity and $\Gamma(y_0)$ is the local circulation at the same location along the span. By integrating the equation over the span of a finite wing, the total lift of the wing can then be obtained:

$$L = \int_{-\frac{b}{2}}^{\frac{b}{2}} L'(y)dy = \rho_\infty V_\infty \int_{-\frac{b}{2}}^{\frac{b}{2}} \Gamma(y)dy \tag{17}$$

From here, the induced drag can be computed by integrating the individual drag elements produced by each vortex filament. The expression for the induced drag per unit span is given by:

$$D'_i = L'_i \sin(\alpha_i) \tag{18}$$

The induced angle of attack, α_i, represents the difference between the global angle of attack, α, and the local or effective angle of attack, α_{eff}. The importance of the induced angle of attack lies in its relationship to downwash and ultimately induced drag. This parameter is central to the proportionality between downwash and induced drag which can be seen clearly by studying the similar triangles in Figure 2.2. Increasing the angle of attack results in an increased induced angle of attack and a corresponding increase in both downwash and a proportionate amount of induced drag.
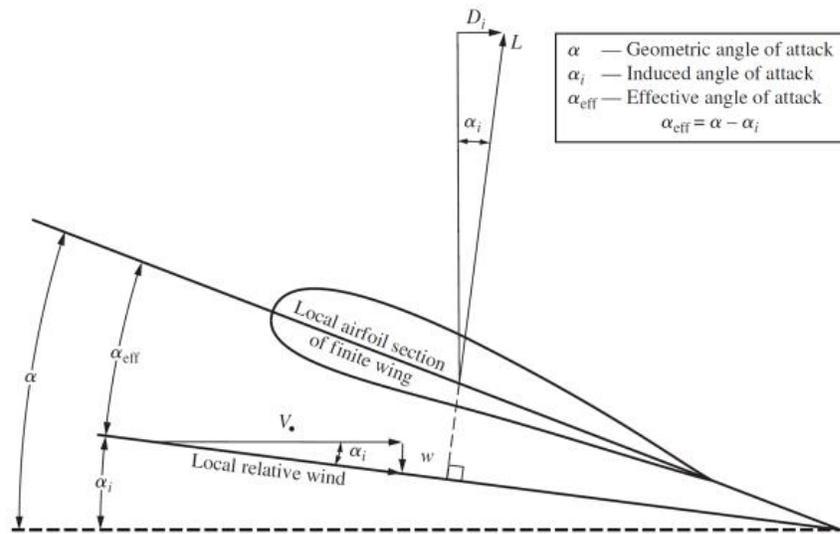
Figure 2.2: Induced angle of attack and associated downwash. [9]

The induced angle of attack is small for the cases considered in this paper so small angle theory can be employed to dismiss the sin function in the expression for induced drag per unit span. The lift force equation can then be substituted for the lift expression (Eq. 17). After adjusting and simplifying, the resulting equation for total induced drag is as follows:

$$D_i = \rho_\infty V_\infty \int_{-\frac{b}{2}}^{\frac{b}{2}} \Gamma(y)\alpha_i(y)dy \tag{19}$$

13

Equations 16-19 are the main aerodynamic parameters of a finite wing that fall out of lifting line theory. They are used in XFLR5 to determine the performance characteristics of the wings studied in this thesis.

2.2 Airfoil Verification

Two-dimensional analysis was performed on each of the two Standard Cirrus airfoils to confirm that later three-dimensional analysis used the correct airfoil geometry. The lifting line method used in this research used the results of the two-dimensional analysis to establish the section lift characteristics of the three-dimensional wing. For that reason, it was important to validate that the airfoil coordinates were faithful to their real geometries. The coordinates for both airfoils were sourced from the Schempp-Hirth sailplane specifications [10], and tested in XFLR5 against the empirical results published in a technical paper about the Standard Cirrus sailplane [8], and in a NACA report of wind tunnel analysis [11].
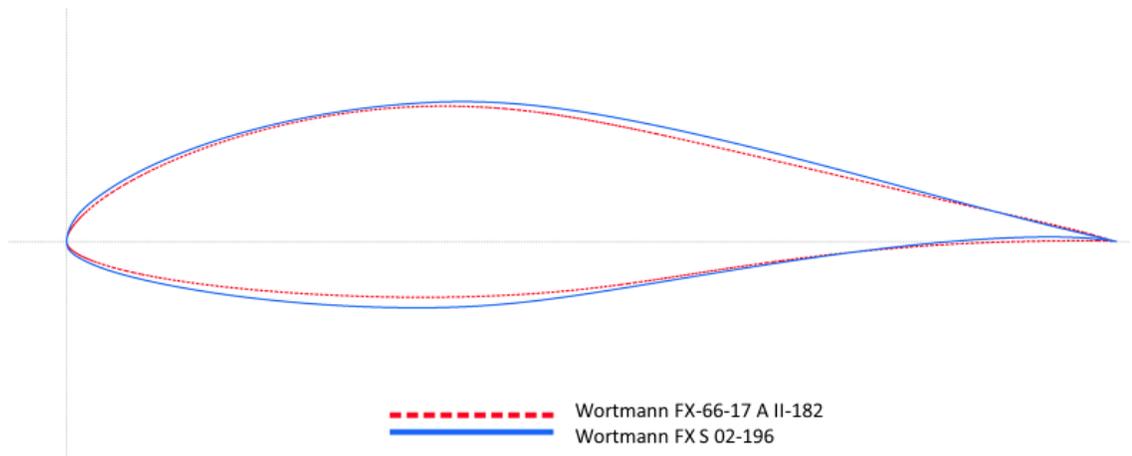
Figure 2.3: A comparison of the two airfoils used on the Standard Cirrus Sailplane drawn over a shared neutral line.

The geometries shown in the above figure are to scale and they illustrate the noticeably thick nature of these low speed laminar airfoils. They were designed for low speed aerodynamics and to trip the flow to transition at a specified point. Some characteristics of the foils are tabulated below for further comparison.

Table 2.1: A tabulated comparison of airfoil characteristics.

Property	Wortmann FX S 02-196	Wortmann FX-66-17 A II-182
Thickness	19.59%	18.21%
Max thickness position	36.14%	35.34%
Max camber	3.65%	3.80%
Max camber position	47.35%	37.54%

The imbedded version of XFOIL within XFLR5 was used to perform the analyses on each of the two airfoils of the Standard Cirrus sailplane. After importing and refining the panels of the airfoil geometries in the program, the analyses were defined by inputting a Reynolds number of 1,500,000 and a Mach number of 0.10 which were selected to simulate the same conditions as those that were used in the comparative experimental studies. A standard N_{crit} value of 9 was selected for the analysis and the airfoils were swept through a range of angles from -3 degrees to +10 degrees to represent those used by the NACA wind tunnel study.

Table 2.2: Parameters used for the airfoil validation study in XFLR5.

Parameter	Value
XFLR5 foil analysis type	1
Re	1,500,000
Mach number	0.10
N_{crit}	9
Number of panels	300
Range of α	-3 to +10
V_0	$26.25 \frac{m}{s}$
ρ	$1.225 \frac{kg}{m^3}$
v	$1.5\text{x}10^{-5} \frac{m^2}{s}$

The results of the analysis indicated that the airfoil geometry taken from the coordinates provided by the Schempp-Hirth specifications were in accordance with the pressure port data recorded in the NACA wind tunnel study. To illustrate this, the discrete data points taken from the wind tunnel test were overlaid on the curves produced by XFLR5 for C_P versus normalized chord location at several angles of attack. This analysis was performed for all the cases provided in the wind tunnel testing with Reynold's number ranging from 0.5×10^6 to 6.0×10^6, Mach numbers from 0.05 to 0.35, and the following angles of attack: -4.05°, -2.00°, 0.00°, 2.03°, 4.00°, 6.07°, 7.07°, 8.05°, 9.18°, 10.16°, 11.23°, and 12.14°. A representative graph of this type at α = 0.00˚ can be seen in Fig 2.3 to confirm that the airfoil pressure field characteristics were validated by the empirical data for the conditions applied in the three-dimensional analysis.
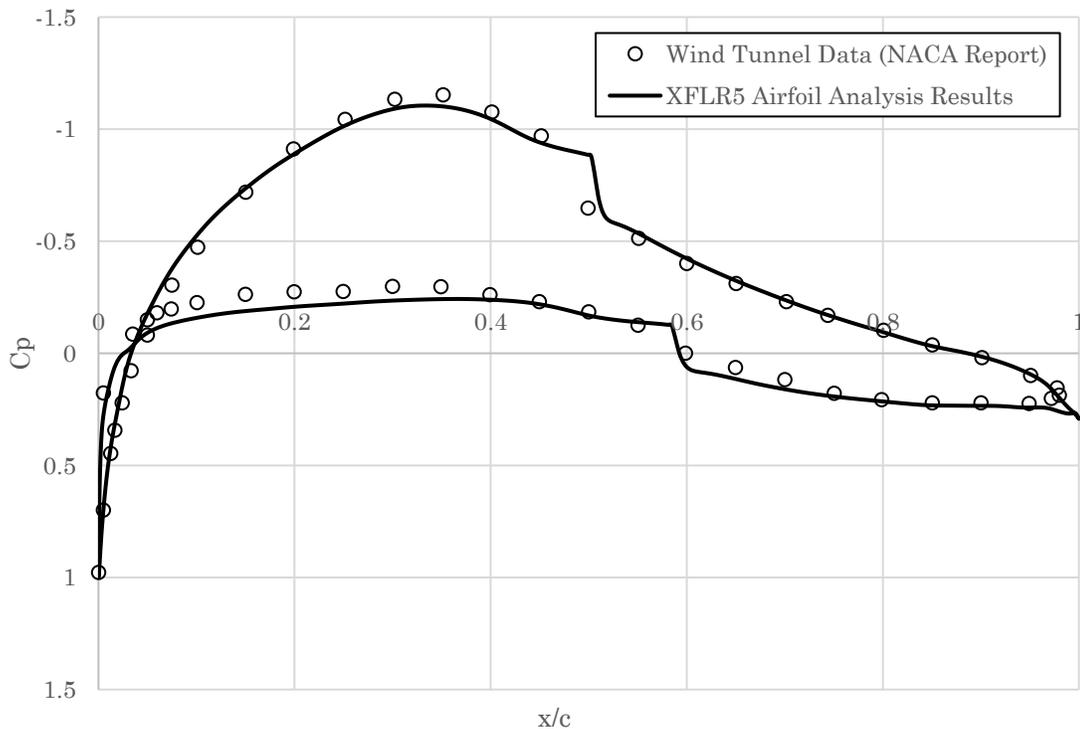
Figure 2.4: XFLR5 results compared against empirical NACA data for root airfoil at α = 0.00˚.

2.3 Baseline Wing Design and Validation

The validated airfoils were used to recreate the Standard Cirrus wing in XFLR5 for establishing a baseline of performance. The geometry of the Standard Cirrus wing was found in the sailplane operator's manual produced by Schempp-Hirth [10]. The wing is composed of a blended combination of the two validated airfoils. From the root chord to the inboard side of the aileron, the wing uses a linear transition between the Wortmann FX S 02-196 and the Wortmann FX-66-17 A II-182. The section from the inboard side of the aileron to the wingtip is entirely made up of the latter airfoil. For simplicity, the aileron control surfaces were not modeled for the analysis.
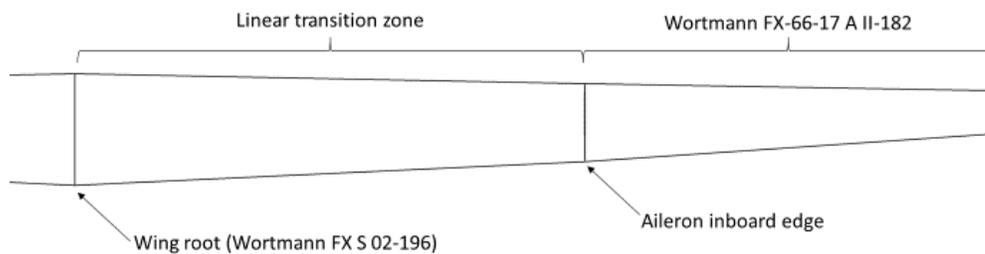
Figure 2.5: Planform view of the Standard Cirrus wing indicating the configuration of the airfoils.

2.3.1 Wing Geometry Definition

The Standard Cirrus wing has a 15-meter wingspan and a wing area of 9.745 square meters. The wing features a dihedral of 3 degrees, a slight sweep of 1.45 degrees, and a washout of 1.5 degrees. These parameters were input to the XFLR5 wing design function on a per wing section basis. This way, the geometry was specified for both the inboard and outboard regions of the wing surfaces. XFLR5 has a default linear transition between airfoils when there exists an aerodynamic twist through a wing section. This allowed for the linear transition zone between root chord and inboard side of the aileron of the Standard Cirrus wing to be faithfully recreated in the program. Henceforth, the modeled Standard Cirrus wing will simply be referred to as the "baseline wing" in this report. For clarity, all data associated with the baseline wing will be color coded blue in all figures and plots.

2.3.2 Panel Refinement Study

After establishing the Standard Cirrus wing geometry in XFLR5, a panel refinement study was carried out to determine the density of panels required to produce convergent results using the lifting line theory method. The panel count was iteratively increased from an initial coarse pattern until the results of the analysis converged onto a consistent value. The coefficient of drag was used as the primary data point to determine convergence given the importance of the parameter to the results of this research. The panel distributions were set to uniform in both the x and y directions because of the square geometry of the Standard Cirrus planform. A table of the panel density settings against the resulting coefficient of drag is provided below.

Table 2.3: Panel refinement study.

Iteration	x-panels	y-panels	CD
1	5	15	0.0095
2	10	30	0.1019
3	20	60	0.1019
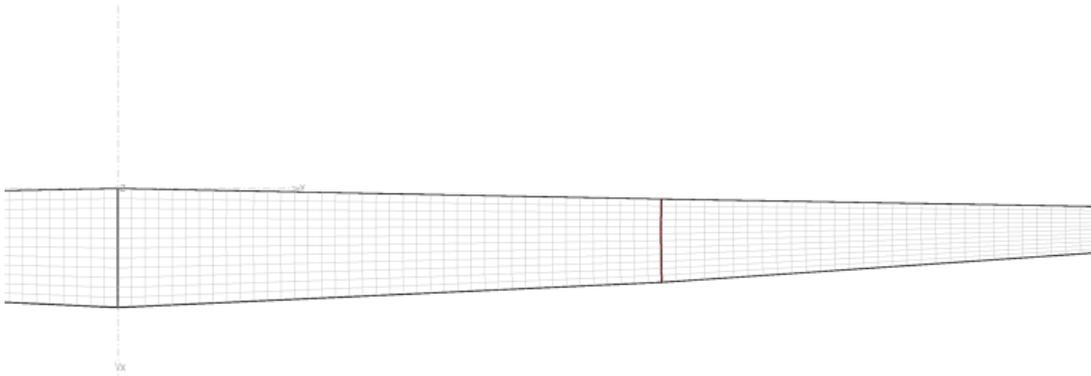
Figure 2.6: Semi-span planform view of the final panel distribution from the refinement study.

2.3.3 Determination of Root Bending Moment

After validating the model against the flight test data, the root bending moment of the baseline wing was determined so that it could be used as the primary constraint in the design of the bell wings. XFLR5 calculates the root bending moment of a wing by integrating the moments about the wing root produced by aerodynamic forces acting along the span of the wing. The plot produced by the program indicated a root bending moment of 2470 Nm and is shown below.
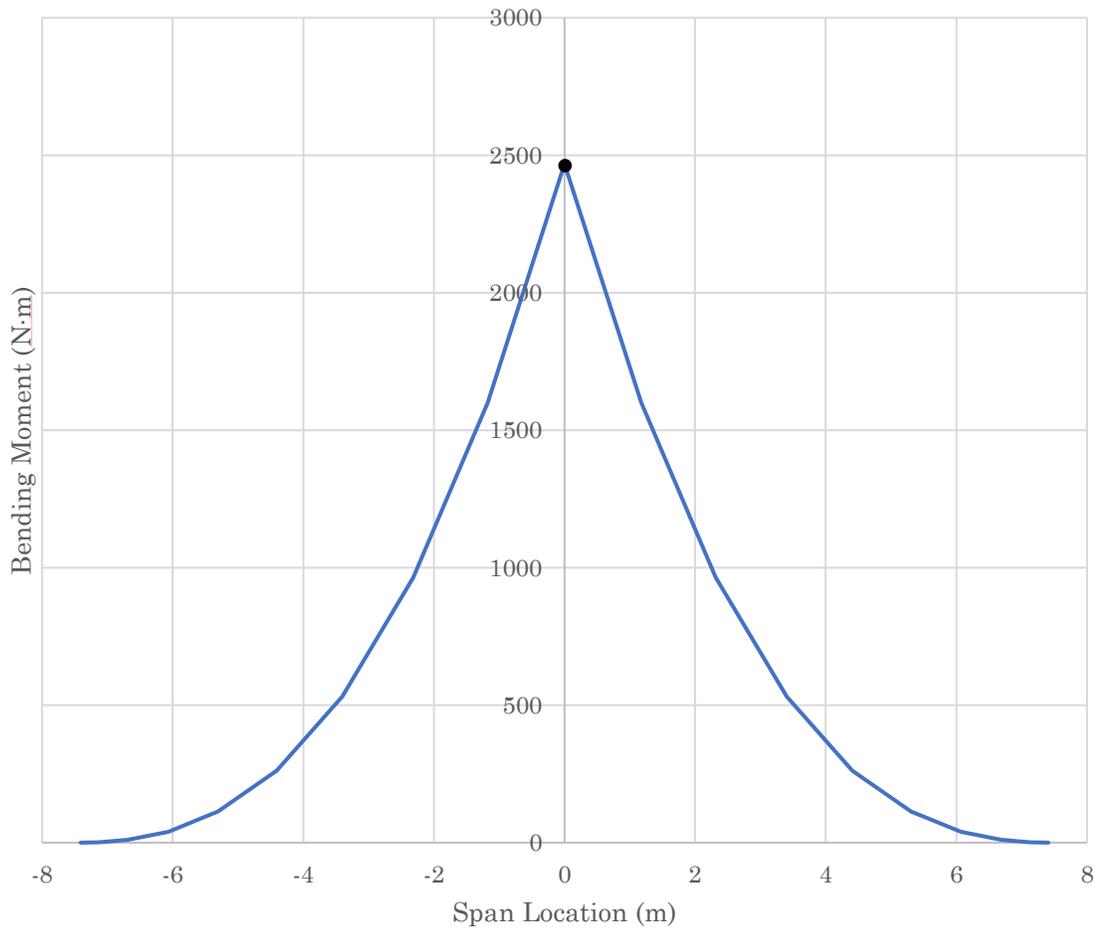
Figure 2.7: Bending moment against wingspan for baseline wing. The root bending moment corresponds to span location of zero.

21

2.3.4 Lift Distribution of the Baseline Wing

For reference the lift distribution of the baseline wing was analyzed in XFLR5 to determine how closely it matched to an ideal elliptical curve. The calculated distribution was plotted on top of an ideal ellipse target curve defined as

$$L(y) = \left[1 - (\frac{2y}{b})^2\right]^{1/2} \tag{20}$$

where *b* is the wingspan [13].
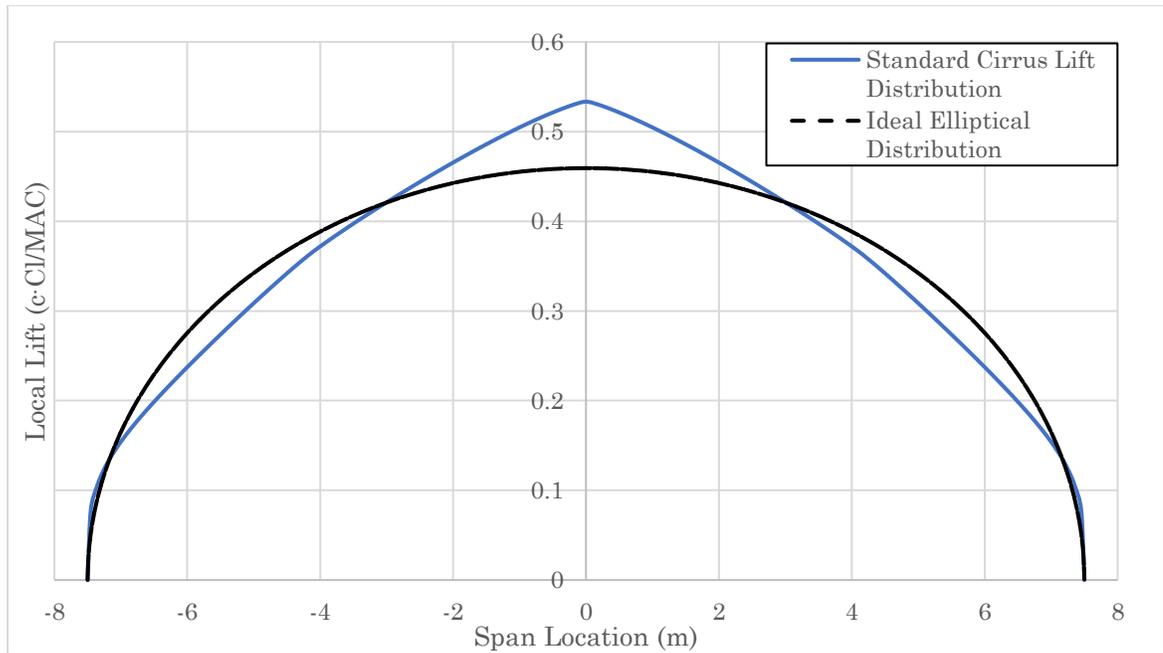
Figure 2.8: Comparison of baseline wing lift distribution versus ideal ellipse distribution.

A cursory assessment of the lift distribution comparison suggests that there is a significant difference between the Standard Cirrus wing and an ideally loaded elliptical distribution. This qualitative discrepancy is primarily a result of differences in configuration between the model and the full Standard Cirrus sailplane. A discussion of the effects of the incongruous lift distributions is provided below.

The baseline wing distribution is greater than the target ellipse around midspan because the aerodynamic effects of the fuselage and empennage of the Standard Cirrus glider are not factored into the analysis. The Standard Cirrus sailplane is configured with an all moving tail

plane that acts to provide longitudinal stability and pitching moment equilibrium. This key component to the sailplane design also possesses associated lift and drag components. The tail plane was designed to induce lift in the downward direction to trim out the pitching moment about the aircraft center of mass. Therefore, the main wing on the Standard Cirrus was intentionally designed with a roughly 6-meter span about the center of the wing that overshoots the ideal elliptical loading guideline. The sum of the positive and negative lift components from the main wing and the tail plane respectively yields a lift distribution that cosmetically fits the ideal ellipse curve more closely. The aerodynamic consequences of investigating the wing apart from the tail plane are insignificant to this research, however, as can be shown by the Oswald efficiency metric.

The span efficiency number (e) is a correction factor that indicates the difference in drag between a given wing and a perfect elliptically loaded wing of equivalent aspect ratio. It is defined as follows [18]:

$$e = \frac{(C_{D,i})\pi AR}{C_L{}^2} \tag{21}$$

where the $C_{D,i}$ term represents the induced drag coefficient. A span efficiency number of 1 corresponds to a perfect elliptical distribution with most conventional aircraft lying in the 0.9-1.0 range [14]. The modeled Standard Cirrus baseline wing was calculated to have an e of 0.96 in XFLR5 which suggests that it was designed to have induced drag characteristics derived from an elliptical distribution. Furthermore, the tail plane has an area of roughly $0.5\ m^2$ which is 5% of the main wing with an area of $10\ m^2$. Using the respective wing areas as the characteristic dimensions for lift and drag calculations, one can conclude that the tail plane does not contribute significantly to the analysis. With a validated baseline wing established, a wing with bell shaped lift distribution was ready to be designed and analyzed.

Chapter 3

BSLD WING DESIGNED WITH VARIED CHORD LENGTH

An iterative design philosophy was adopted for this task by first constraining as many geometry parameters as possible. The primary constraint drew from the original formulation of the bell-shaped lift distribution which placed a constraint on the bending moment of the wing. To preserve the integrity of the comparison between simulated wings, the bending moment of the modeled baseline wing was taken as the primary constraint used in the design of bell wings. This left three principle parameters to adjust along the wingspan in order to create the desired bell lift distribution: chord length, geometric twist, and aerodynamic twist.

3.1 Bell Wing from Adjusted Chord Lengths

For design simplicity, the first attempted bell wing was created by only adjusting chord lengths along the span of the wing. Properties of the wing geometry from the baseline wing were preserved wherever possible to maintain continuity in the comparison. These properties included dihedral angle, sweep angle, root chord length, and airfoil transitions along the wingspan. The wingspan itself was left unconstrained however to match the root bending moment of the bell wing with that that of the baseline wing.

Starting with the original planform of the baseline wing, chord lengths were adjusted until the resulting lift distribution took on the ideal bell-shape. XFLR5 includes an option that allows for a target lift distribution curve to be overlaid on the distribution plot produced by the wing analysis. The target curve was set to:

$$L(y) = \left[1 - \left(\frac{2y}{b}\right)^2\right]^{3/2} \qquad (22)$$

in the program which corresponds to the bell-shaped lift distribution specified in the Prandtl theory [15]. After arriving at an approximate distribution that matched the target template, the bending moment was determined for that wing. If it was below the target root bending moment, then the wingspan was increased, and the iterative chord adjustment process was repeated until a wing with the correct lift distribution and root bending moment was arrived at. Additional panels were included on the wing as necessary to provide sufficient adjustable chord lengths to arrive at a lift distribution that followed the curvature of the target bell curve. The resulting wing had a root bending moment of 2460 Nm (within 1% of the baseline wing), and a span of 16.8 meters or 11.3% longer than the baseline wing. Despite an increase in wingspan, the total wetted area of the wing decreased by 6.5% to 9.115 m^2. A semi-span planform is provided in the figure below. For ease of reference, data associated with the chord varied bell wing were represented in green color coding. This wing was also referred to as simply bell wing in further discussions unless clarification was required in context.
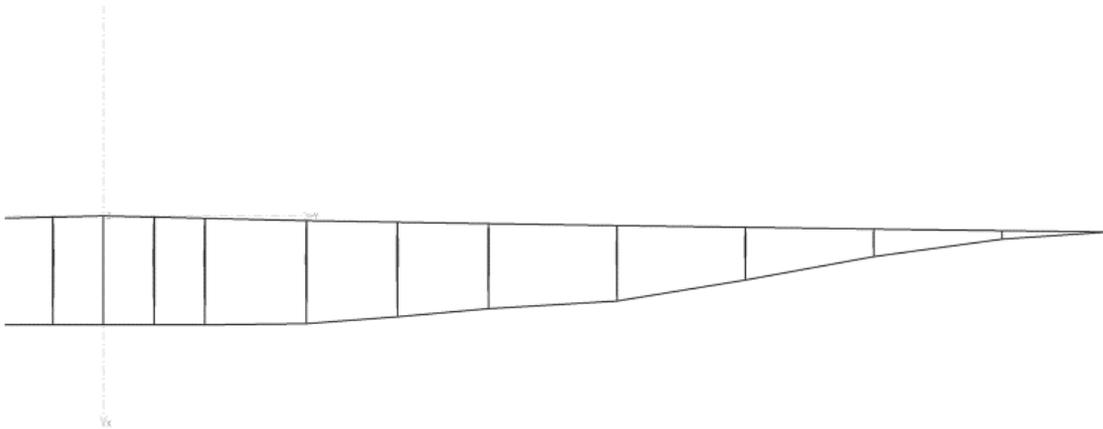
Figure 3.1: Semi-span planform of the bell wing created by adjusting chord lengths. The leading edge is towards the top of the figure.

3.2 Paneling and Analyzing the Bell Wing

A similar paneling method and panel density was adopted for the bell wing as the baseline wing. The narrow wingtips presented a challenge during this step however, because the panels at in the outboard most section of the wing were skewed in order to fit the geometry. This complication was mitigated by adjusting the panel distribution to mesh as smoothly as a possible with the adjacent section, but the analysis results still reflected discontinuities in the wingtip region. This is consistent with expectations of the analysis method however, because the lifting line theory is limited by highly tapered wing geometries.

A fixed velocity lifting line analysis was used to analyze the bell wing because it allowed for a cruising speed to be specified. The other analysis parameters pertaining to flight conditions were preserved from the baseline wing analysis in the previous chapter. A table of these parameters is provided below.

Table 3.1: Parameters used for the Bell Wing Analysis in XFLR5.

Parameter	Value
XFLR5 analysis type	Fixed velocity LLT
Re	$1.00\text{x}10^3 \sim 1.59\text{x}10^6$
V	$26.25\,\frac{m}{s}$
ρ	$1.225\,\frac{kg}{m^3}$
v	$1.5 \times 10^{-5}\,\frac{m^2}{s}$

The analysis failed in the wingtip region at around 85% semi-span as mentioned before because the Reynolds number there dropped below the envelope that was established in the two-dimensional airfoil analysis. The lift distribution produced by XFLR5 reflects the subtle wingtip discontinuity and can be seen in the following plot with the target distribution represented by the dashed line. Detail of the paneling and geometry of the wingtip section shown in the figure directly below.
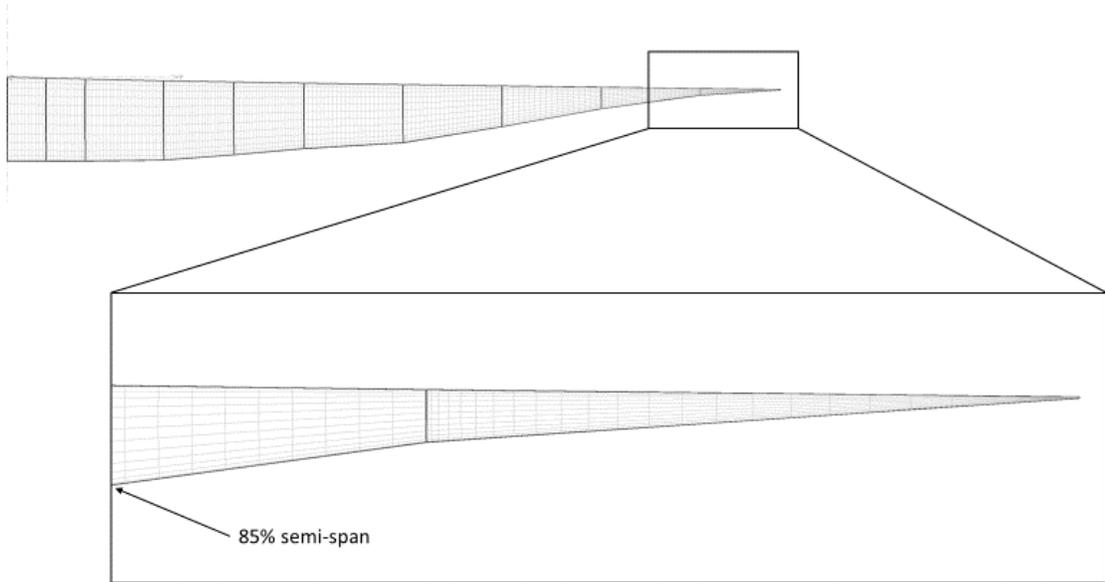
Figure 3.2: Detail of wingtip paneling and highly tapered geometry.
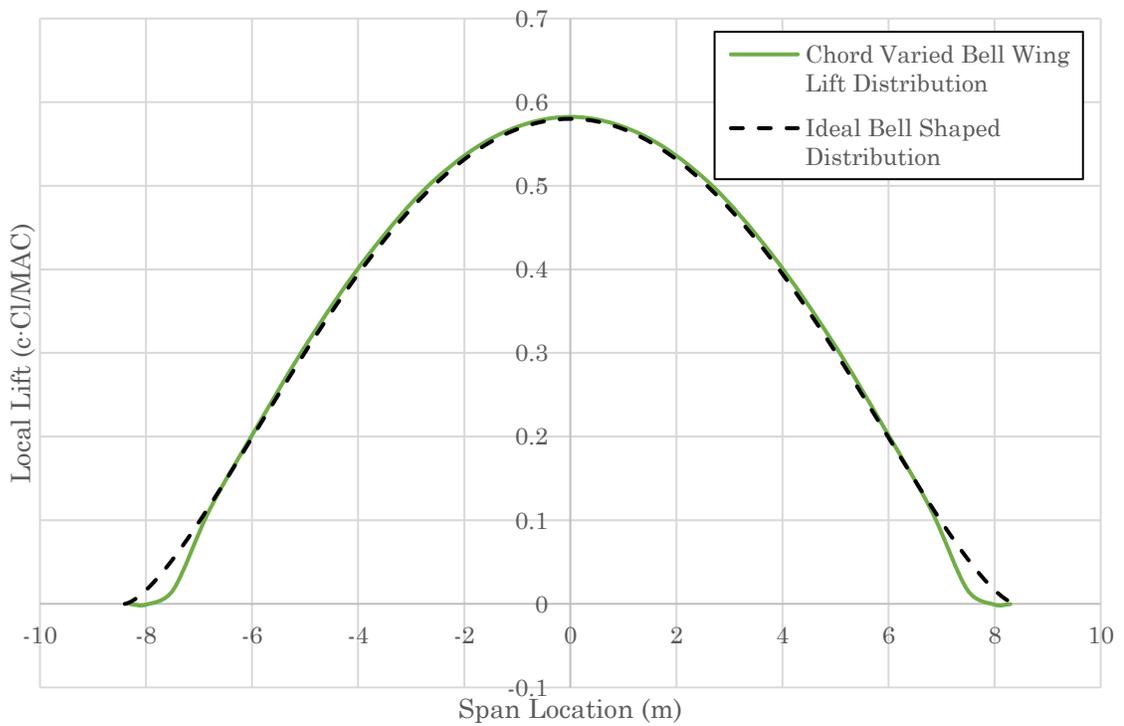
Figure 3.3: Bell wing lift distribution plotted over the target bell curve.

3.3 Comparison of the Bell Wing and the Baseline Wing

With the analyses completed, characteristics of interest between the chord varied bell wing and the baseline wing were compared. The following metrics were used: CD_i, C_L, C_D, C_L/C_D, wingspan, wing area, AR, and wing loading.

Table 3.2: Comparison of performance characteristics between the baseline and bell wing analyses.

metric	baseline	bell
$C_{D,i}$	0.0024	0.0029
C_L	0.411	0.447
C_D	0.0102	0.0113
C_L/C_D	40.3	39.6
Wingspan	15.0 m	16.8 m
Wing Area	9.745 m^2	9.115 m^2
AR	23.1	31.0
Wing Loading	30.8 $\frac{kg}{m^2}$	33.0 $\frac{kg}{m^2}$

Based on the tabulated data, the bell wing has a 2.0% worse lift to drag ratio, and a higher induced drag coefficient. The overall lift coefficient for the bell wing is greater owing to the decrease in wing area, but that difference did not result in better lift-to-drag ratio because of the added overall drag. In order to achieve the bell lift distribution while maintaining the same root chord and bending moment as the baseline wing, the bell wing required a 12% increase in wingspan. This figure is contrary to the Bowers paper that claims the bell wing of matching root bending moment should occur when the wingspan is increased by 22% [15]. Despite an increase in wingspan, the bell wing features a 6.5% decrease in wing area due to the strongly tapered wingtips. Finally, assuming that both wings have a mass of 300kg, the bell wing has greater wing loading owing to the decreased wing area. It should be noted, however, that the bulk of the load

is carried near the root and that the wings become unloaded at around 70% span. This effect can be seen in the following plot comparing the induced drag coefficient versus span for both the baseline and bell wings. The induced drag coefficient is defined as

$$C_{D,i} = \frac{D_i}{2\rho V^2 S}.$$

(23)

where the induced drag force D_i, is the expression derived in equation 19. The plot also illustrates the discontinuity from the limitations of lifting line theory in the highly tapered wingtip regions of the bell wing. Furthermore, the chart illustrates the deviation of the baseline wing from a true elliptical induced drag distribution. In the case of a truly elliptically loaded wing, the expected induced drag/downwash curve is a constant single value across the whole span.
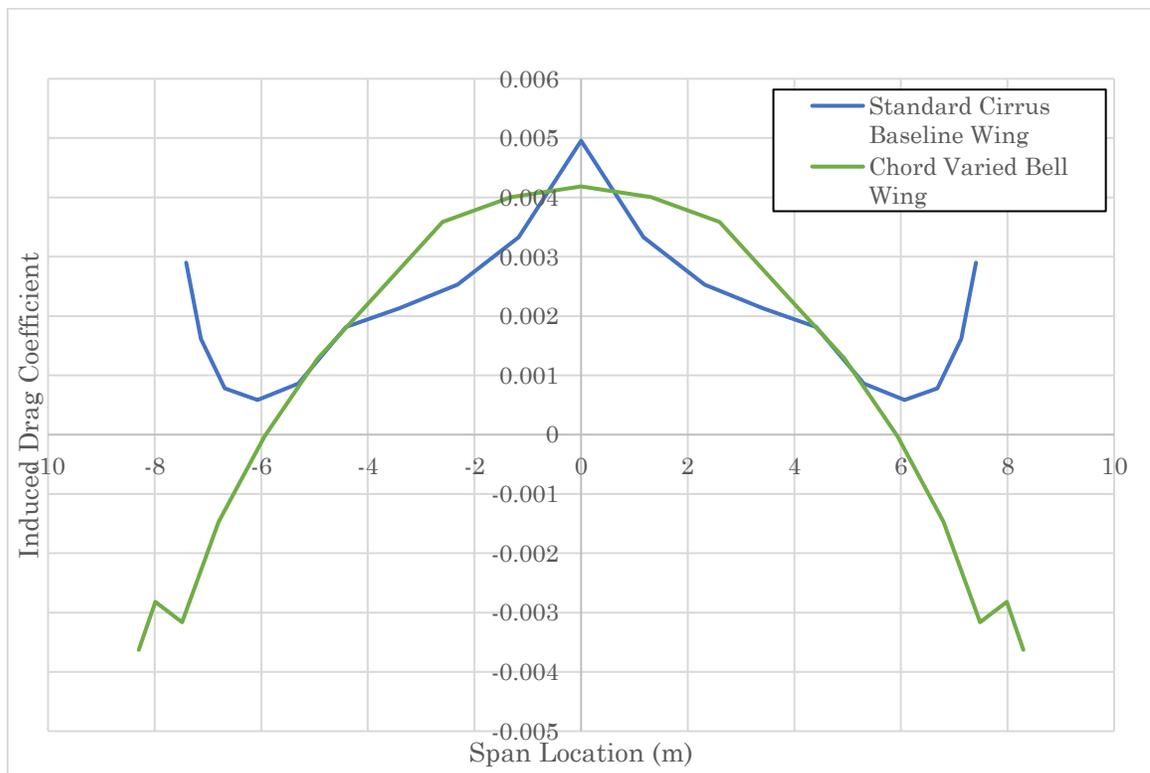
Figure 3.4: A comparison of induced drag coefficient versus wingspan for the baseline and bell loaded wings.

Chapter 4

BSLD WING DESIGNED WITH GEOMETRIC TWIST

4.1 Bell Wing from Geometric Twist

A second bell wing was designed using geometric twist to remedy the problems stemming from the highly tapered wingtip geometry of the first attempt. The bell wing resulting from strictly varying chord length along the span provided insight into the performance of a wing with the specified lift distribution, but the geometry was not practical. The wingtips tapered to a single point at a severe angle in the last section of wing which presented problems in analysis. Furthermore, such a wing would present unreasonable manufacturing challenges if a bell wing of this type was ever built. The results of substituting geometric twist for chord variation as a method of defining lift distribution are investigated in the following section. The data featured in the following plots resulting from analysis for this wing are color coded in red.

Like the design method used to create the first bell wing, an iterative approach was adopted to build in geometric twist with XFLR5. The same initial geometry constraints on dihedral angle, sweep angle, root chord length, and airfoil type along the wingspan were carried over from the baseline wing. Then, starting with a 15m wingspan, geometric twist was added to the wing until the lift distribution matched the target curve defined in the previous section. At this point, the root bending moment of the wing was determined and compared against the constraint of 2470 Nm carried over from the baseline wing. The initial attempt at designing the second bell wing yielded too small a root bending moment, so the wingspan was extended iteratively while adjusting twist angle at wing sections until both the bending moment and lift distribution requirements of the wing were met. The completed bell wing had wingspan of 16.8 meters, a bending moment of 2440 Nm (within 1% of the targeted value), and the following lift distribution.
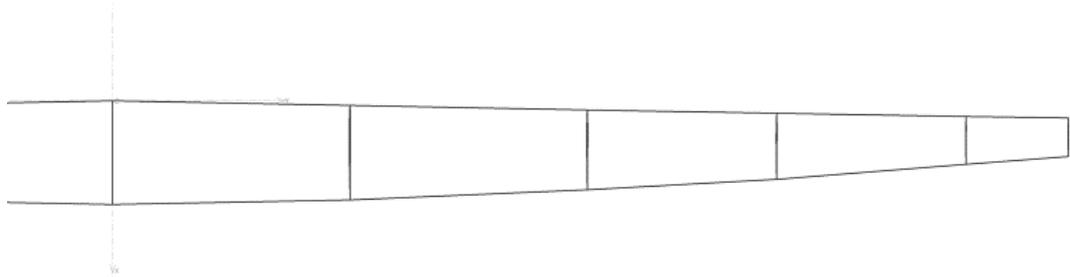
Figure 4.1: Semi-span planform of the bell wing created by adjusting geometric twist. The leading edge is towards the top of the figure.
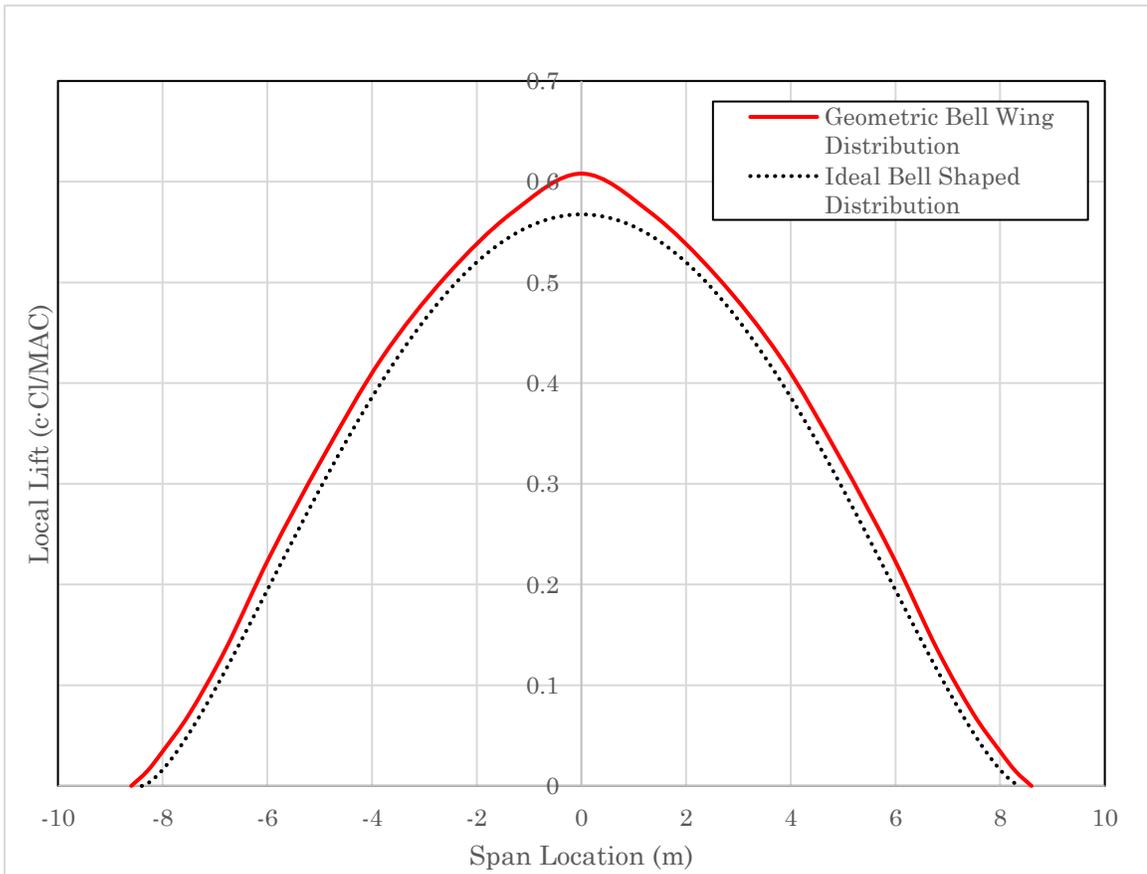
Figure 4.2: Geometric bell wing lift distribution plotted over the target bell curve.

Unlike the lift distribution produced for the chord varied bell wing, the geometric bell wing slightly overshoots the ideal bell-shaped target curve over the span of the entire wing. This resulted from the limited resolution in the wing design tools provided in XFLR5. Both the root bending moment and the total lift produced by the wing were required to meet target values while the geometric twist angles were varied at each wing section. Unlike the simpler one-dimensional adjustment of chord lengths used for the first bell wing, adjustment of geometric twist required the XFLR5 program to interpolate in multiple dimensions between wing section stations. Small variations in twist angle near the root propagated out towards the wingtips. This led to greater variation in overall lift distribution and a tendency to overshoot the target curve when the root chord was held constant with respect to the baseline wing.

The wing used in the analysis has a higher overall CL than the target curve. The overshoot is most pronounced at the root of the wing where the modeled wing has a 5% higher local lift. The discrepancy tapers to a value of 3% at 1-meter outboard of the root and remains at the level to the wingtip. The overshoot on the local lift of the modeled geometric bell wing is therefore less than 5%. While the analyzed induced drag values were inflated by a similar amount from this discrepancy, the shape of the induced drag distribution was still accurately reflected in Fig 4.1 because the overshoot was systematic. Thus, the aerodynamic nature of the drag from this wing could still be interpreted confidently.

4.2 Comparison of the Bell Wing with Geometric Twist and the Baseline Wing

After creating a wing that met the design requirements, performance characteristics were once compared against those of the baseline wing. The same metrics were tabulated as in the previous section and then added in a new column.

Table 4.1: Comparison of performance characteristics between the baseline and geometric bell wing analyses.

metric	baseline	bell	geometric bell
CD_i	0.0024	0.0029	0.0020
C_D	0.0102	0.0113	0.0095
C_L	0.411	0.447	0.346
C_L/C_D	40.3	39.6	36.3
Wingspan	15.0 m	16.8 m	16.8 m
Wing Area	9.745 m^2	9.115 m^2	11.3 m^2
AR	23.1	31.0	25.0
Wing Loading	30.8 $\frac{kg}{m^2}$	33.0 $\frac{kg}{m^2}$	25.6 $\frac{kg}{m^2}$

The geometric bell wing featured a 20% drop in the induced drag coefficient but also had a lower lift to drag ratio. This can partly be explained by a 14.8% increase in wetted area over the chord-varied bell wing which decreased the lift coefficient by a corresponding amount. The remaining difference in lift-to-drag performance must then have stemmed from other sources of drag such as skin friction. A later section assesses the amount of added skin friction and changes in lift and drag forces from the different wing geometry. The wingspan that yielded the desired lift distribution and root bending moment was equivalent to the span of the first bell wing at 16.8m. The aspect ratio was only 8% greater than the baseline wing compared to the greater increase observed with the first bell wing. The increase in area corresponded to a 18.4% lighter wing loading assuming a mass of 300 kg.

While the overall drag coefficients are of comparable magnitude between the three wings, the lift coefficient exhibits a larger range. The lift coefficient for the geometric bell wing is 15.8% less than that of the baseline wing. Consideration of the definition of the lift coefficient sheds light on the source of this decrease:

$$C_L = \frac{2L}{\rho V^2 S} \tag{25}$$

Where S stands for the reference surface area of the wing in question. The other terms in the equation are constant between the wings by virtue of the constrained analysis parameters. Therefore, the increased wing area required to achieve the bell lift distribution through geometric twist has a significant detriment to the lift coefficient. This increase in wing area also creates more skin friction which counteracts the savings on induced drag.

The chord varied bell wing has a decreased wing area however, which factored into the 8.8% increase in lift coefficient over the baseline. Given the tradeoffs between the chord variation and geometric twist design methods, the most aerodynamically efficient configuration is likely a hybrid bell wing that incorporates elements from both types of geometry variation. The chord varied wing could benefit from using geometric twist at the wingtip to avoid the thin taper while the geometric twist wing could benefit from shorter chord lengths along the span to reduce skin friction and increased wing area. The result would be a more manufacturable wing with less induced and skin friction drag than the baseline.
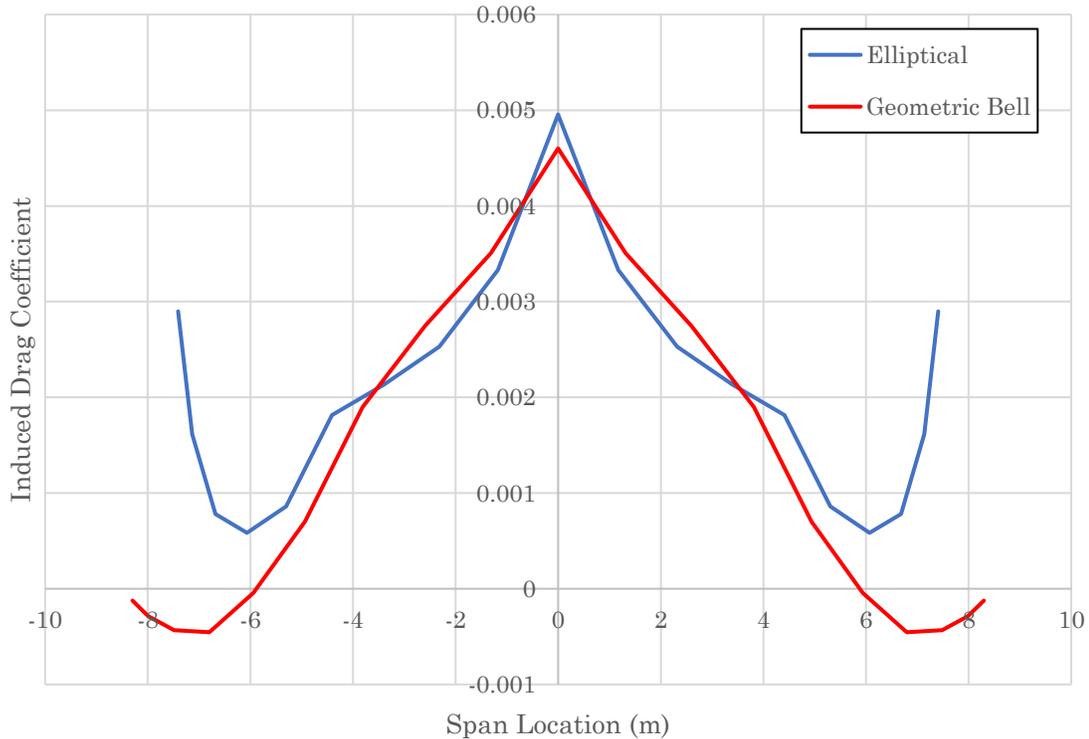
Figure 4.3: Comparison of induced drag against span location for baseline versus geometric bell wings

The induced drag is similar for both the baseline and geometric bell wing from the root out to 6 meters along the span. At 6 meters to the wingtip, the trend for induced drag clearly diverges with the baseline wing increasing rapidly while the geometric bell gradually dips below the horizontal axis and then tending towards zero at the wingtip. These trends are consistent with the theory put forward by Bowers [15] where he states that there should be induced thrust expected at around the 70% span location for bell shaped lift distributions. The first bell shaped wing with chord variations exhibited a similar feature also around the 6-meter mark which corresponds to 71.4% of span – consistent with the established theory.

The significance of the unloaded wingtips can be interpreted in several different ways. First, in contrast with the baseline wing, the bell wings exhibit a gradual and continuous change in induced drag and therefore circulation over the span of the wing. Elliptically loaded wings have a sharp discontinuity at the wingtip where the strong wingtip vortices appear which call for the

application of winglets. According to these results, a bell-loaded wing would have no need for wingtip devices because it does not redirect energy into a vortex. Additionally, a bell wing could be designed with a control surface in the unloaded region of the wing to allow for the potential of coordinated turns with less or no rudder input from a vertical surface in the empennage. Negative induced drag can be interpreted as induced thrust and so it follows that an aileron in that region of the bell loaded wing would produce a yaw moment in the coordinated direction as the intended roll direction when deflected. A reduction in the size of the rudder in the empennage assembly of an aircraft with a bell-loaded wing could further reduce total airplane.

4.3 Comparison of Baseline and Geometric Bell Speed Polars

For further comparison, the speed polars of the baseline and geometric bell-shaped wings were overlaid on the same plot. The speed polar is an effective tool for analyzing the efficiency of a sailplane. It was included in this report because the baseline wing was derived from a sailplane and so this representation of data can aid in the understanding of the differences in modeled geometric bell wing. Due to the complications in analysis with the wingtip region of the first bell wing, its speed polar data was not included.
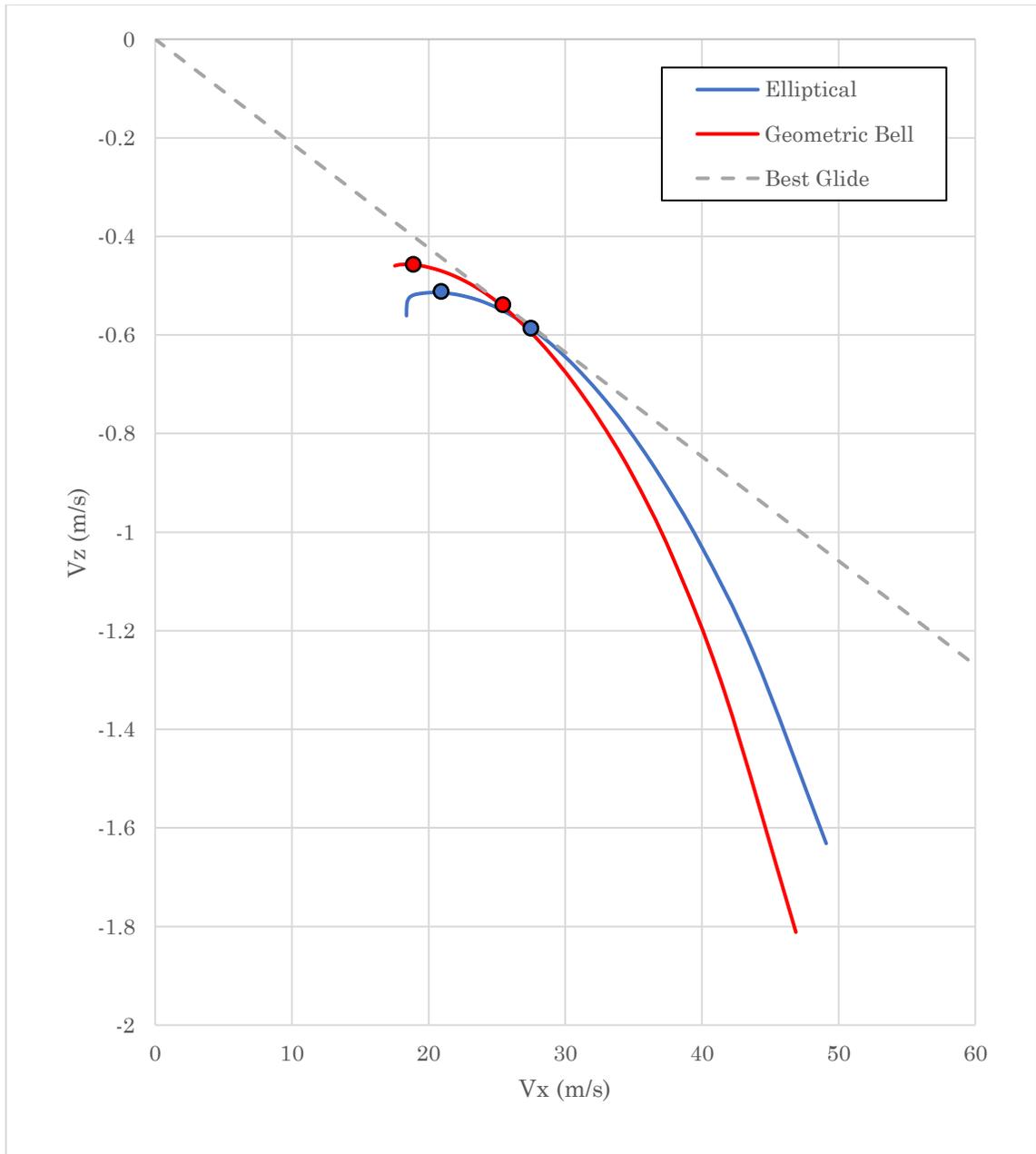
Figure 4.4: Comparison of speed polars for the baseline and geometric bell wings with the shared best glide line superimposed. Minimum sink and tangent points are indicated with color coded markers.

The vertical axis represents the rate of sink (Vz) across a range of airspeeds (Vx). At different airspeeds, the wings sink at different rates depending on their geometries and aerodynamic characteristics such as lift distribution. The speed polar is a useful tool for determining the best speed to fly to minimize the sink rate for a given wing configuration. It also graphically represents

37

the best achievable glide ratio for a glider and what airspeed and sink rate are associated with that metric.

The speed polars for the two wings have the same best glide slope of 43 though that occurred at a speed of 25 m/s for the geometric bell wing and slightly faster around 27 m/s for the baseline wing. These slopes were determined by finding the angle subtended by the horizontal axis and the line tangent to the polar curves. The minimum sink values are found at the maxima of the polar curves and for the geometric bell wing was slightly better than baseline wing at -0.45 m/s versus -0.5 m/s. The glide performance of the geometric bell wing falls off at a faster rate than the baseline wing at higher speeds. At first blush, it appears that the bell wing would be better suited to less energetic soaring days if it were ever purposed for sailplane applications because it performs better at lower airspeeds. In contrast, the baseline wing maintains a lower sink rate at higher airspeeds, so a sailplane with this wing could cover more ground without sacrificing as much altitude.

Chapter 5

ESTIMATION OF DIFFERENCES IN DRAG FORCES BETWEEN WINGS

5.1 Induced Drag Calculations

Up to now, the differences in induced drag between the wings has been considered from the standpoint of the drag coefficients. While this form of comparison is good for developing a sense of the magnitude to which different forms of drag contribute to the overall drag of the wing, an analysis of the induced drag force provides a clearer picture of how the wings compare to each other. The induced drag forces were calculated using the following definition:

$$D_i = \frac{1}{2}\rho V^2 S(CD_i) \tag{26}$$

where CD_i represents the induced drag coefficients calculated by XFLR5 in the previous chapter. The results of this calculation applied to each of the analyzed wings is tabulated below.

Table 5.1: Comparison of induced drag forces.

	Baseline	Bell	Geometric Bell
CD_i	0.0024	0.0029	0.0020
S	$9.745\ m^2$	$9.115\ m^2$	$11.30\ m^2$
D_i	$9.991\ N$	$11.08\ N$	$9.479\ N$

The drag force induced by the chord varied bell wing is 10.3% greater than the baseline wing and the 5.3% less drag is induced by the geometric bell wing. This sets the stage for an investigation into the magnitude of skin friction drag that each of these wings produces.

5.2 Skin Friction Analysis

The lifting line analysis of the geometric bell wing indicated that it induces 5.3% less drag than the baseline wing. This was at the cost of a 14.8% increase in wing area however, so a flat plate turbulent skin friction comparison was conducted to estimate the additional viscous drag

produced by the greater surface area. This analysis was performed for geometric bell wing and the baseline wing by approximating the wings with flat plates of equivalent mean aerodynamic chord. For the bell wing with varied chord however, the wing was broken into multiple sections to account for the highly tapered outboard sections.

5.3 Governing Equations and Methodology

The method for estimating skin friction was adapted from J. Anderson's *Fundamentals of Aerodynamics* in his coverage of incompressible flow over airfoils [16]. It is intended to provide an order-of-magnitude accurate estimation of the amount of skin friction produced by a wing in fully turbulent flow. From empirical data, the skin friction drag for incompressible turbulent flow over a flat plate is expressed by

$$C_f = \frac{0.074}{Re_c^{0.074}} \tag{27}$$

where Re_c represents the Reynolds number based on chord length. Given their lightly tapered geometries, the mean aerodynamic chord was used for the calculations of skin friction drag for the baseline wing and the geometric bell wing.

$$Re_c = \frac{\rho_\infty * V_\infty * MAC}{\mu_\infty} \tag{28}$$

The overall skin friction was calculated from the coefficient of skin friction drag by integrating over the associated wing area and multiplying by the dynamic pressure of the freestream.

$$D_{sf} = \int_{wing\ surface} C_f \frac{\rho V^2}{2} dA = SA_{wing} * C_f * \frac{\rho V^2}{2} \tag{29}$$

For the chord varied bell wing, the same methodology was used over three sections as indicated in the following figure to account for the taper near the wingtips.
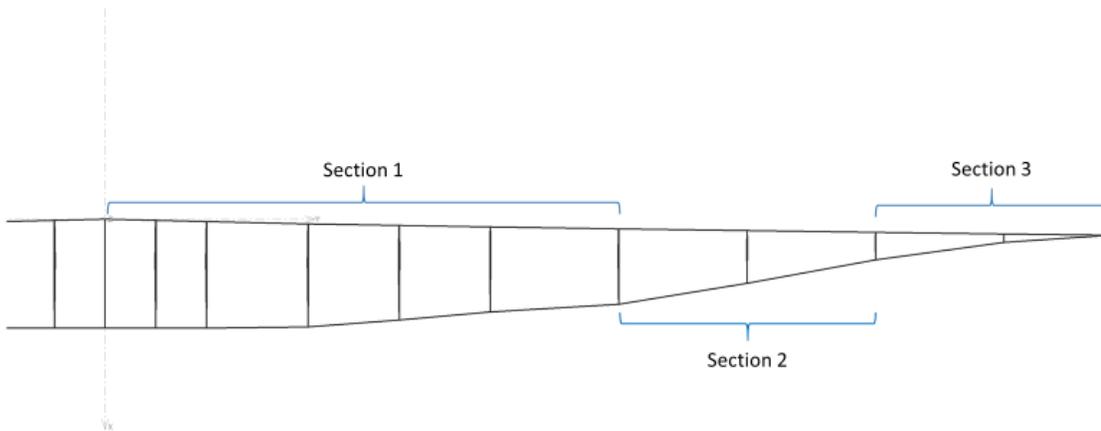
Figure 5.1: Sections used for the estimation of skin friction for the chord varied bell wing

5.4 Results

The differences in skin friction drag between the three studied wings are discussed here. The coefficients of skin friction for the baseline and geometric bell wings were within 1% of each other owing to similarly dimensioned mean aerodynamic chords. This meant that the total skin friction essentially scaled with direct relation to their proportions in wing area. The geometric bell wing had 14.8% greater surface area which translated to 15% higher skin friction in comparison to the baseline wing.

After breaking the chord varied bell wing into the three sections and calculating for each one, it was found to induce 6.2% less skin friction than the baseline wing. This decrease in drag is proportional to the difference in wetted area between the two wings of 6.5%. The results of these calculations are summarized in the following table along with the results of the induced drag force calculations.

Table 5.2: Comparison of coefficients of drag and drag forces

	Baseline	Chord Varied Bell	Geometric Bell
C_f	9.00×10^{-3}	9.01×10^{-3}	8.93×10^{-3}
D_{sf}	$37.0\ N$	$34.7\ N$	$42.6\ N$
CD_i	0.0024	0.0029	0.0020
D_i	$9.991\ N$	$11.08\ N$	$9.479\ N$

At the flight parameters defined for this research, the skin friction component of the overall drag factors in around four times greater than the induced drag component. Given that the wings in this analysis all share the same root bending moment and total lift force, the savings in induced drag provided by the geometric bell wing do not outweigh the increased skin friction drag that arises from the increased wing area. This further analysis reinforces the potential benefits of a wing with bell shaped loading designed with a hybrid combination of chord variation and geometric twist. The table above indicates that the chord varied bell wing had less skin friction drag but the induced drag was increased by 10% over the baseline wing. The strength of the geometric bell lies in the reduction of induced drag however at the sacrifice of skin friction efficiency. A combination of the two configurations could optimize both sources of drag a yield a higher performing wing given the same initial constraints and flight data.

Chapter 6

DISCUSSION OF RESULTS

This chapter examines how the results of this research compare with the results of similar past studies including Prandtl's original findings about the aerodynamic efficiency of a bell-shaped wing loading. In other research, different approaches to conducting a comparison between lift distributions produced varying conclusions about the performance of bell-shaped lift distributions. Among the reviewed papers, two key characteristics of theoretical bell wings were commonly quoted for their characterization: wingspan and reduction in induced drag both published as percentages of an ideal baseline. These figures of merit for both the literature-reviewed bell wings and the geometries studied in this thesis are in the following table.

Table 5.3: Comparison of changes in wingspan and induced drag between multiple studies of bell-shaped lift distributions. Italicized results refer to those from this report.

Bell Wing Name	Wingspan % Increase Over Elliptical Baseline	Induced Drag % Reduction Over Elliptical Baseline
Original Prandtl/Bowers [2], [15]	22.5%	11.1%
Klein & Viswanathan 1973 [5]	33%	15.6%
Klein & Viswanathan 1975 [6]	16%	7.1%
Chord Varied Bell Wing	12%	-10.4%
Geometric Twist Bell Wing	12%	5.3%

The data presented in the table represent the results of solving the same problem with different initial constraints and methodologies. In the case of the chord-varied bell wing, there is a net increase in total induced drag. This result does not follow the trend of the rest of the other research and likely stems from the issues encountered with XFLR5 in the wingtip region of the wing geometry. Interestingly, the geometric twist bell wing produced results that most closely match those of the 1975 Klein & Viswanathan paper. Their conclusion was reached by placing

43

initial constraints on the integrals of the spanwise shear force and bending moment distributions. Of the reviewed papers, this approach was the most thorough and considered the most factors contributing into wing structural weight.

To put the results of this research in context, the limits of the methodology must be reiterated. Firstly, the simulations were run only for steady state conditions modeled after those that a Standard Cirrus glider would commonly fly in. The wings were also only analyzed at zero degrees of angle of attack. These parameters were chosen to simplify the comparison so that a fundamental understanding of the differences between the lift distributions could be taken away from the work. Therefore, the conclusions drawn about the induced and skin friction drag components only apply to the prescribed flight conditions. Different aircraft attitudes and air data could lead to alternative conclusions about the aerodynamic performance of the wings.

Furthermore, as mentioned in earlier parts of the report, the lifting line method in XFLR5 presented challenges relating to the chord varied bell wing geometry. The chord length at wing tips was too short for the airfoil analysis tool to include in the envelope for the three-dimensional simulations. The short chord length resulted in a Reynolds number that lay outside of the range of two-dimensional foil data and so the wing performance at the wingtips could not be properly calculated by the software using the specified method. So, the aerodynamic results for the chord varied bell wing are unreliable and the induced drag force was overestimated because the discontinuity at the wingtip imitated a wingtip vortex. Perhaps the vortex lattice method would be better suited to solving for the unusual geometry presented by this wing.

The bell wings studied in this thesis were designed with only chord variation and geometric twist. While the reviewed papers suggest that there are wings of bell-shaped lift distribution that would significantly reduce induced drag, they do not define the geometry of such a wing. It was determined through this work that the design approach to wings with bell loading can yield results with variable amounts induced and skin friction drag from incongruous wing areas. Future research could consider incorporating aerodynamic twist in addition to chord variation and geometric twist to optimize a wing with the target bell distribution. Such a wing

44

would draw on the wing area reducing benefits of chord variation, while exploiting the geometric twist for improved ability to analyze and manufacture the model.

More complex geometries would require closer consideration of the effects of viscous flow. XFLR5 was selected for this application because of its simplicity and suitability to produce lift and drag data from laminar affects. Once a more mature understanding of how different wing geometries alter lift distribution and induced drag is reached, specified designs requiring investigation of viscous characteristics should then be studied further with CFD. That will enable a much more detailed understanding of how skin friction factors into overall drag calculations among different bell wings.

A normalized plot of the reviewed lift distributions was also produced for direct qualitative comparison. In the same style as the Klein & Viswanathan paper, both axes were normalized to provide a more intuitive picture. The semi-spans on the horizontal axis were normalized against the wingspans of each respective wing. The local lift distributions on the vertical axis were normalized against the root lift distribution for each respective wing.
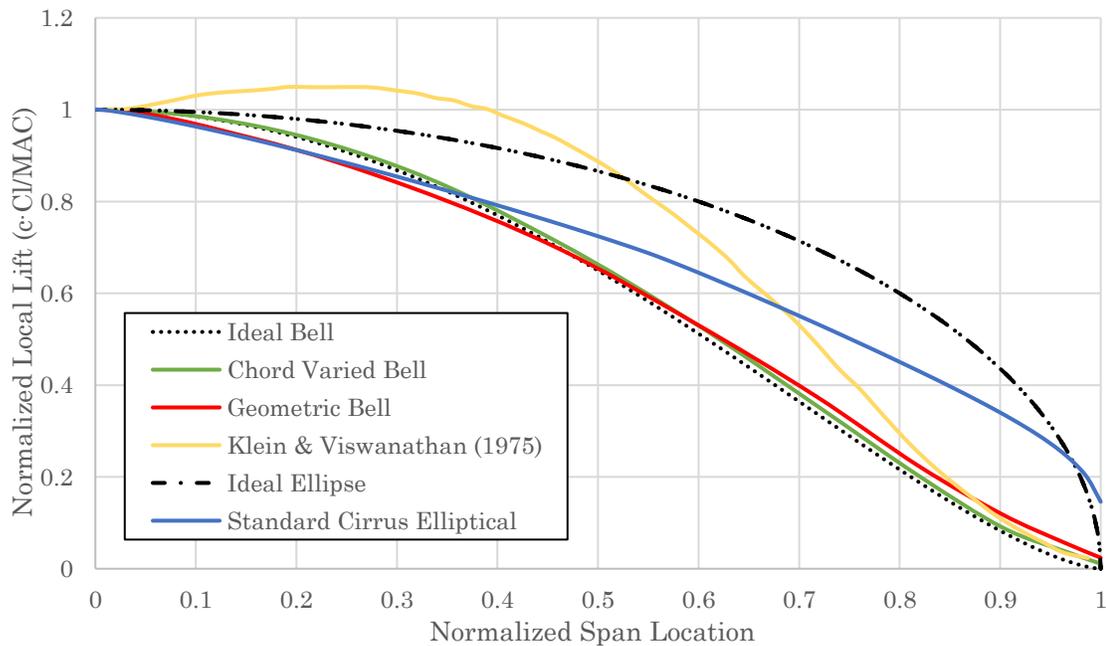
Figure 6.1: Normalized comparison of the studied lift distributions

Chapter 7

CONCLUSION

XFLR5 was used to perform a one-to-one comparison between wings with bell-shaped lift distribution and an elliptically loaded baseline wing modeled after the Standard Cirrus sailplane. Results of interest include the changes made to the baseline wing geometry to produce the desired lift distribution, and the reduction in induced drag. The results of this study were compared to other research that carried out the same comparison but with alternative methodology.

The first major conclusion was that analyzing a chord-varied bell wing using the lifting line method provided by XFLR5 was not workable. The geometry tapered severely enough at the wingtip that the Reynolds number reached a value that could not be covered in the two-dimensional airfoil batch analysis. Furthermore, such a geometry was concluded to be impractical because manufacturing such a wing would be challenging considering how the wingtip is thin and narrow and converges to a single point. Due to the issues that arose with wingtip section there were few conclusions about the performance of the bell-shaped lift distribution that could be drawn from its analysis. Surprisingly, the wetted area of the resulting bell wing was 6.5% smaller than the baseline wing despite having a 12% longer wingspan.

The bell wing with geometric twist had a more amenable geometry in XFLR5 and demonstrated a 5% reduction in induced drag and a 12% increase in wingspan over the baseline wing. This result does not agree with the original Prandtl theory which stated an 11% reduction with a 22% increase in wingspan. The discrepancy lies in the different approaches taken between methods where root bending moment was constrained in this paper as opposed to consideration of how the local spar weight contributes to local bending moment. Of the reviewed information on the subject, the results from XFLR5 analysis match most closely with those found in the 1975 Klein & Viswanathan paper which claims a 7.1% reduction in induced drag corresponding to a 16% increase in wingspan.

The increase in wingspan and wing area resulted in a corresponding 15% increase in skin friction for the specified simulation conditions. This outweighs the savings in induced drag threefold and points to importance of considering all contributions to overall drag when designing a wing based on a specified lift distribution. It also highlights the pros and cons of utilizing different wing design parameters such as chord variation and geometric twist. The chord varied wing had less wing area than the baseline but higher induced drag – the opposite effect to using purely geometric twist. An aerodynamic efficiency optimized bell wing will need to incorporate some combination of these design elements.

Considering that there are large number of parameters that can be adjusted when designing a wing with bell-shaped lift distribution, it is conceivable that there are an equally diverse number of possible wings each with their own characteristics. Given the results of the bell wing from this paper and the other reviewed resources however, it appears that there are certain aerodynamic benefits to using a bell-shaped wing loading if the designer is able to design around total wing structure in some way rather than around a constrained span.

This thesis only provides a surface level understanding of the aerodynamic performance of wings with bell-shaped lift distributions. Further research into viscous effects is necessary for a more comprehensive analysis of total drag. The analysis performed in this study indicated that the additional area of the bell wing with geometric twist increased the skin friction by 15% over the baseline. This additional drag might negate the benefit of using the bell distribution but a CFD or wind tunnel study would provide a more conclusive answer to that question.

BIBLIOGRAPHY

[1] Ludwig Prandtl. Applications of Modern Hydrodynamics to Aeronautics, *NACA Report No. 116*,1921.

[2] Ludwig Prandtl. Uber Tragflugel kleinsten induzierten Widerstandes. *Zeitschrift fur Flugtechnik und Motorluftschiffahrt*, 24:557-561, 1933.

[3] Lennart Batenburg. Modeling the Performance of the Standard Cirrus Glider using Navier-Stokes CFD. *Technical Soaring*, 38(1):5, 2014.

[4] R.T. Jones. The Spanwise Distribution of Lift for Minimum Induced Drag of Wings Having a Given Lift and A Given Bending Moment, *NACA Technical Note 2249*, 1950.

[5] Armin Klein and S.P. Viswanathan. Minimum Induced Drag of Wings with Given Lift and Root Bending Moment, *Kruze Mitteilungen – Brief Reports*, 1973.

[6] Armin Klein and S.P. Viswanathan. Approximate Solution for Minimum Induced Drag of Wings with Given Structural Weight, *Journal of Aircraft* 12(2): 124-126, 1975.

[7] W.F. Philips, D.F. Hunsaker, and J.J. Joo. Minimizing Induced Drag with Lift Distribution and Wingspan, *Journal of Aircraft* 56(2) 431-441, 2019.

[8] Thomas Hansen. Modeling the Performance of the Standard Cirrus Glider using Navier-Stokes CFD. *Technical Soaring*, 38(1):5-14, 2014.

[9] John D. Anderson Jr. Prandtl's Classical Lifting Line Theory, *Fundamentals of Aerodynamics,* 5th Edition: 424-426, 2011.

[10] Schempp-Hirth. Control Surface Movements, *Flight and Service Manual for the Sailplane - Standard Cirrus-,* 16, 1970.

[11] Dan M. Somers, Experimental and Theoretical Low-Speed Aerodynamic Characteristics of a Wortmann Airfoil as Manufactured on a Fiberglass Sailplane, *NASA Technical Note D-8324,* 1977.

[12] Rein I. Hoff and Guy B. Gratton, Estimating Sailplane Mass Properties, *Technical Soaring,* 34(4): 118-125, 2010.

[13] John D. Anderson Jr. Prandtl's Classical Lifting Line Theory: Elliptical Lift Distribution, *Fundamentals of Aerodynamics,* 5th Edition: 430, 2011.

[14] John D. Anderson Jr. Three-Dimensional Incompressible Flow, *Fundamentals of Aerodynamics,* 5th Edition: 503, 2011.

[15] Albion H. Bowers, Robert "Red" Jensen, Brian Eslinger, and Christian Gelzer. On Wings of Minimum Induced Drag: Spanload Implications for Aircraft and Birds, *NASA Technical Publication-2016-219072*, 2016.

[16] John D. Anderson Jr. Estimating Skin-Friction Drag: Laminar Flow, *Fundamentals of Aerodynamics,* 5th Edition: 372, 2011.

[17] Ajith V.S., Ravikumar Paramasivam, and K. Vidhya. Study of Optimal Design of Spar Beam for the Wing of an Aircraft, *IJEDR,*5(3): 179-193, 2017.

[18] Mark Drela. AVL User Primer, *MIT Aero & Astro,* web.mit.edu/drela/Public/web/avl/avl_doc.txt, 2017.

APPENDIX A: Airfoil Coordinates [10]

Wortmann FX S 02-196

	Chord	Upper	Lower		Chord	Upper	Lower
1	1.00000	.00000	.00000	29	.37059	.13327	-.06255
2	.99893	.00026	.00019	30	.33928	.13218	-.06317
3	.99572	.00106	.00069	31	.30866	.12981	-.06292
4	.99039	.00234	.00146	32	.27886	.12639	-.06198
5	.98296	.00411	.00233	33	.25000	.12207	-.06048
6	.97347	.00637	.00318	34	.22221	.11695	-.05846
7	.96194	.00912	.00386	35	.19562	.11108	-.05599
8	.94844	.01238	.00429	36	.17033	.10455	-.05312
9	.93301	.01616	.00439	37	.14645	.09747	-.04992
10	.91573	.02048	.00412	38	.12408	.08993	-.04646
11	.89668	.02535	.00346	39	.10332	.08202	-.04280
12	.87592	.03076	.00238	40	.08427	.07384	-.03898
13	.85355	.03671	.00085	41	.06699	.06540	-.03504
14	.82967	.04314	-.00117	42	.05156	.05679	-.03098
15	.80438	.05000	-.00367	43	.03806	.04822	-.02682
16	.77779	.05722	-.00666	44	.02653	.03996	-.02256
17	.75000	.06469	-.01012	45	.01704	.03201	-.01827
18	.72114	.07234	-.01403	46	.00961	.02395	-.01410
19	.69134	.08007	-.01837	47	.00428	.01553	-.01004
20	.66072	.08779	-.02308	48	.00107	.00723	-.00561
21	.62941	.09539	-.02811	49	.00000	.00000	.00000
22	.59755	.10276	-.03335				
23	.56526	.10977	-.03871				
24	.53270	.11628	-.04405				
25	.50000	.12212	-.04922				
26	.46730	.12703	-.05395				
27	.43474	.13068	-.05793				
28	.40245	.13280	-.06083				

Wortmann FX 66-17 A II-182

	Chord	Upper	Lower			Chord	Upper	Lower
1	1.00000	.00000	.00000		30	.33928	.12873	-.05319
2	.99893	.00016	.00016		31	.30866	.12706	-.05293
3	.99572	.00105	.00036		32	.27886	.12405	-.05218
4	.99039	.00263	.00051		33	.25000	.11985	-.05099
5	.98296	.00484	.00062		34	.22221	.11461	-.04943
6	.97347	.00755	.00068		35	.19562	.10851	-.04753
7	.96194	.01062	.00069		36	.17033	.10169	-.04531
8	.94844	.01391	.00065		37	.14645	.09426	-.04281
9	.93301	.01754	.00047		38	.12408	.08635	-.04004
10	.91573	.02151	.00013		39	.10332	.07805	-.03702
11	.89668	.02578	-.00035		40	.08427	.06948	-.03379
12	.87592	.03038	-.00105		41	.06699	.06076	-.03035
13	.85355	.03534	-.00203		42	.05156	.05201	-.02674
14	.82967	.04076	-.00341		43	.03806	.04339	-.02295
15	.80438	.04662	-.00522		44	.02653	.03490	-.01911
16	.77779	.05282	-.00744		45	.01704	.02665	-.01528
17	.75000	.05934	-.01011		46	.00961	.01902	-.01137
18	.72114	.06614	-.01327		47	.00428	.01201	-.00759
19	.69134	.07316	-.01695		48	.00107	.00584	-.00373
20	.66072	.08032	-.02114		49	.00000	.00069	.00069
21	.62941	.08755	-.02579					
22	.59755	.09477	-.03073					
23	.56526	.10189	-.03574					
24	.53270	.10876	-.04046					
25	.50000	.11512	-.04460					
26	.46730	.12061	-.04792					
27	.43474	.12488	-.05036					
28	.40245	.12770	-.05198					
29	.37059	.12897	-.05290					

APPENDIX B: XFLR5 Wing Design Parameters

Baseline Wing

	y (m)	chord (m)	offset (m)	dihedral(°)	twist(°)
1	0.000	0.910	0.000	3.0	0.001
2	4.173	0.636	0.081	3.0	0.001
3	7.500	0.354	0.138		-1.501

Chord-Varied Bell Wing

	y (m)	chord (m)	offset (m)	dihedral(°)	twist(°)
1	0.000	0.910	0.000	3.0	0.00
2	0.425	0.900	0.010	3.0	0.00
3	0.850	0.890	0.020	3.0	0.00
4	1.700	0.860	0.040	3.0	0.00
5	2.462	0.790	0.053	3.0	0.00
6	3.225	0.710	0.065	3.0	0.00
7	4.300	0.630	0.081	3.0	0.00
8	5.375	0.440	0.096	3.0	0.00
9	6.450	0.230	0.110	3.0	0.00
10	7.525	0.070	0.124	3.0	0.00
11	8.400	0.001	0.134		0.00

Geometric Bell Wing

	y (m)	chord (m)	offset (m)	dihedral(°)	twist(°)
1	0.000	0.910	0.000	3.0	0.00
2	2.087	0.830	0.041	3.0	-0.25
3	4.173	0.700	0.081	3.0	-0.50
4	5.837	0.580	0.110	3.0	-1.75
5	7.500	0.420	0.138	3.0	-3.20
6	8.400	0.340	0.150		-4.00

APPENDIX C: List of Terms

D_i − induced drag

ρ_∞ − freestream density

V_∞ − freestream velocity

b − wingspan

w − induced downwash velocity

y − span location

α_i − induced angle of attack

L − total lift

r − radius of gyration

σ − ratio of elliptical wingspan to bell wingspan

M_R − root bending moment

L' − Local lift force

D'_i − local induced drag

Γ − local circulation

α_{eff} − effective angle of attack

α − angle of attack

e − span efficiency number

AR − aspect ratio

$C_{D,i}$ − coefficient of induced drag

C_L − total coefficient of lift

v − kinetmatic viscosity

Re − Reynolds number

C_D − total coefficient of drag

S − reference area

C_f — skin friction coefficient

MAC — mean aerodynamic chord

D_{sf} — drag from skin friction